THE THERMAL STABILITY OF HYDROGEN-BURNING SHELLS

by

ILMO ROBERT VON RUDLOFF
B.Sc., University of Victoria, 1982

A THESIS SUBMITTED IN PARTIAL FULFILLMENT

OF THE REQUIREMENTS FOR THE DEGREE OF

MASTER OF SCIENCE

in the Department

of

Physics

ACCEPTED
FACULTY OF GRADUATE STUDIES
[redacted]
DEAN
DATE Jan 29, 86

We accept this thesis as conforming
to the required standard

[redacted]
D. A. VandenBerg

[redacted]
F. D. A. Hartwick

[redacted]
J. A. Burke

[redacted]
B. L. Ehle

[redacted]
D. D. Olesky

University of Victoria

September, 1985

Supervisors: Adjunct Assistant Professor Don A. VandenBerg
Professor F. D. A. Hartwick

Abstract

The thermal stability of hydrogen-burning shells in low-mass stars typical of globular clusters has been investigated. A significant tendency towards instability is found to occur as they evolve into red giants, at a location on the colour-magnitude diagram where some globular clusters exhibit a peculiar gap. Heavy-element content, and to a lesser extent, mass and helium abundance are found to affect the degree of instability, through their effects on the temperature dependence of the energy generation rate in the shell. None of the models studied were found to be unstable; however some speculations are offered as to how further destabilization could occur.

Examiners:

[redacted]

D. A. VandenBerg

[redacted]

F. D. A. Hartwick

[redacted]

J. A. Burke

[redacted]

B. L. Ehle

[redacted]

D. D. Olesky

Table of Contents

List of Tables

List of Figures

Acknowledgements

The author would like to thank D. A. VandenBerg and F.D.A. Hartwick for their continued support, enthusiasm, and constructive criticism throughout the preparation of this thesis, and M. Schwarzschild for some timely advice.

1. Introduction

The comparison of stellar models with observations of stars and star clusters continues to be one of the most useful ways of improving our understanding of the physics which controls the structure of stars. VandenBerg (1983), for instance, has demonstrated that the simplest spherically-symmetric, non-rotating models (albeit with the most up-to-date opacities, equation-of-state, and nuclear physics) have surface properties which resemble those observed in most globular cluster stars to a remarkable degree of accuracy. However, as the observations become more refined, some mysteries are revealed. A good example is illustrated in Figure 1, which is a colour-magnitude diagram (CMD) of the globular cluster NGC 288 (the data are taken from Buanonno et al., 1984). Another good example is NGC 6752 - see for example Cannon (1984). Globular clusters are very useful congregations of stars to study because they are very populous (typically 10^5 to 10^7 stars) and their stars appear to be of a uniform age, roughly 15×10^9 years. Before commenting on the peculiarities which are present, it is useful to recall the correspondence of the main features in the CMD with present understanding of stellar evolution.

For most of a star's life, energy generation occurs solely in the core, where the temperature and density is high enough to facilitate nuclear fusion of hydrogen into

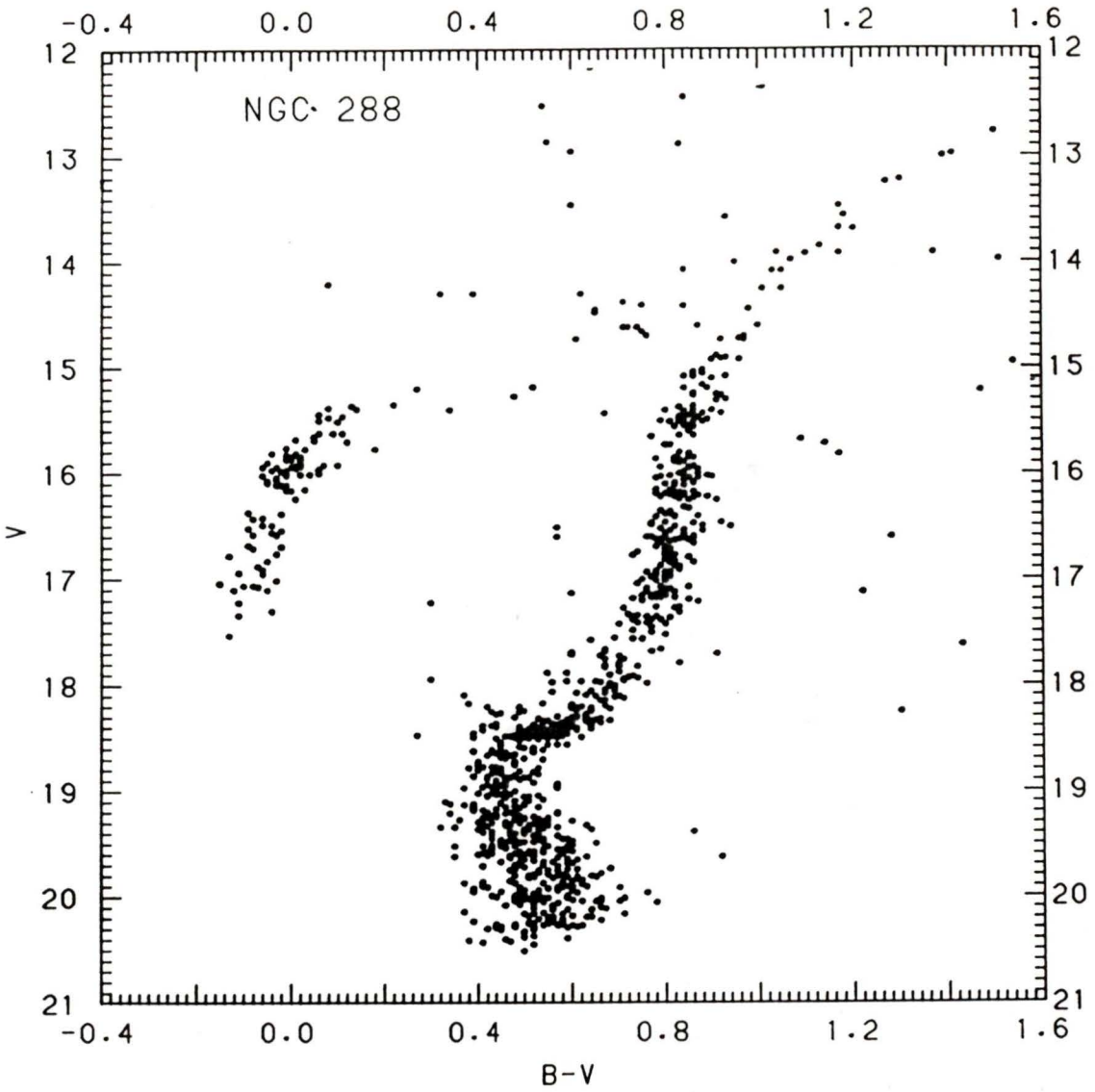

Figure 1: Colour-Magnitude Diagram for NGC 288. The data were taken from Buonanno et al. (1984). B-V is a colour index, which is a measure of stellar temperature: the larger the value the redder and cooler the star is. V is related to the absolute magnitude M_V (that which would be observed at a 10 pc. distance) by $V=M_V+5\mathrm{Log}(r)-5+A$, where r is the distance in pc. and A is the absorption correction. See also Figure 6.

helium (by the p-p chain for stars with masses $< 1.2\ M_\odot$ such as those to be considered here, and by the CNO cycle for higher mass stars). As the core exhausts its supply of hydrogen, however, the growing fraction of helium in the core results in an increase in the mean molecular weight. This would cause a pressure deficiency, so to maintain hydrostatic equilibrium the core must contract. This increases the temperature and density in the central regions, resulting in an increase in the burning rate and an enlargement of the region where fusion can occur. When the centre is finally depleted of hydrogen, the region surrouding it is hot enough to continue burning hydrogen via both the p-p chain and the CNO cycle: this is a hydrogen-burning shell.

The evolutionary phase described thus far is called the main sequence, and corresponds in Figure 1 to the stars with V magnitudes $\gtrsim 18.5$. The masses of the stars determine their luminosity and thus position on the sequence. The faintest, lowest-mass stars burn hydrogen so slowly that they have not evolved significantly since their formation. Those stars at the bluest point of the sequence ($V \sim 18.5$), the turnoff point, are believed to be just at the stage of core hydrogen exhaustion while those still brighter (and redder) are now supported by hydrogen shell burning.

As shell burning proceeds, the core grows in mass as the hydrogen surrounding it is converted into helium by the

shell and continues to slowly condense. The core temperature continues to increase, although at a slow rate as the pressure supporting the dense core material is due more and more to degenerate electrons. In the meantime, the hydrogen-rich outer envelope of the star is expanding and cooling at the surface. Convection becomes the energy transport mechanism for the bulk of this envelope, because the opacity (or radiation absorption) in the cool outer layers is so large.

Helium ignition in the core eventually occurs for all but the lowest-mass stars, as contraction raises the temperature in the core from roughly 10^7 to 10^8 K. This ignition is known as the helium flash. The long curved locus going up from the main sequence represents the shell hydrogen-burning phase just descibed and is called the Red Giant Branch (hereafter RGB). The tip of the RGB marks the approximate point where the helium flash occurs.

Subsequent to the helium flash, the star settles down on the Horizontal Branch (hereafter HB) where both core helium burning and shell hydrogen burning produces the energy which is radiated. In NGC 288 the HB consists primarily of the bright stars bluer than B-V $\sim$ 0.2. The helium-burning core evolves in a manner quite similar to the previous hydrogen-burning core, converting helium into carbon via the triple-alpha process, but exhausts itself much more rapidly. When this occurs, a helium-burning shell

is formed above the inert carbon core, thus resulting in a second shell source. This again moves the star upwards and to the right on the CMD, onto the Asymptotic Giant Branch (AGB) just to the left of the RGB.

Present stellar models are able to predict the gross features of CMDs quite well. With improved observations, however, it has become apparent that the distributions of stars along the RGB and the HB are not smooth: note the gaps at V ~ 17.8 and 16.3, respectively. This suggests that stars must evolve very rapidly through these locations on the CMD so that the chance of observing stars there is very small. Up to now, no satisfactory explanation has been found for these anomalous features - for example, the latest mixing hypothesis by Armandroff and Demarque (1984) was found not to be consistent with the data.

Previous studies of the stability of shell sources

One possible explanation for what is occurring at these evolutionary stages is some kind of instability in the star. Schwarzschild and Härm (1965, hereafter SH) unexpectedly found that helium-burning shells in stars on the AGB of low- to intermediate-mass ($\lesssim$ 1.2 $M_\odot$) may become thermally

unstable. They showed by simple theoretical considerations that if, in a very thin energy generation shell, the temperature dependence of the nuclear burning rate, U, defined by

$$\epsilon \propto T^{U}, \qquad (1)$$

is much greater than about 10, instability should occur. This is the case for the helium triple-alpha burning process and probably for hydrogen burning via the CNO cycle, but not for hydrogen burning by the p-p chain (U has values of about 40, 20 and 4 in these three cases respectively).

According to SH, what happens physically is that when a thin shell expands somewhat, the density in the shell is significantly reduced while the pressure is hardly affected since the weight of the outer layers has not been altered appreciably. By the ideal gas law, $P \propto DT$, the decrease in D will be accompanied by an increase in T which serves to increase the energy generation rate, ϵ. The star will respond to the higher ϵ by further expanding the shell, thus creating a positive feedback cycle. The higher the temperature dependence of the energy generation, the more likely and dramatically this will occur. The two most important conditions favoring this kind of instability[1] are that, if a thermal perturbation occurs, the shell be thin enough to not affect the hydrostatic structure of the star yet be thick

enough so as to not radiate away too quickly the excess heat generated.

To confirm their understanding and to rule out computational artifacts, SH introduced into their computer code a routine to test the thermal stability of model stars. This involved the conventional first-order perturbation method, with the time dependence of all perturbations assumed to be exponential, i.e.,

$$\text{perturbation} \propto e^{t/\tau} \tag{2}$$

where τ is a real number, being positive or negative depending on whether or not a perturbation grows or is damped out with time. Indeed SH found a positive growth perturbation with an e-folding time (i.e. the time over which the magnitude has grown by a factor of e) of order 10^6 years occurring some 10^8 years after the helium flash.

In a subsequent study, Härm and Schwarzschild (1972, hereafter HS) came back to the subject to consider oscillatory instabilities (i.e. complex eigenvalues) and to study their formation and growth in model stars. Again studying only helium-burning shells, they found that real positive growth perturbations evolve from stable oscillatory solutions.

Dennis (1971) studied the matter in the same manner for a 15 $M_\odot$ star, and found no positive instability. Radiation

pressure was shown to be a stabilizing factor, and in stars greater than 5-15 $M_\odot$ it guarantees their thermal stability.

Bolton and Eggleton (1973, hereafter BE), using very simplified analytical models of both hydrogen and helium shells, found that hydrogen-burning shells should become unstable and oscillatory when U rises to above ~12, and purely unstable when U is above ~23.

Are any of these results supported by observations? The first consequence of the instability would be an increase in ϵ and a general adiabatic expansion of the shell. SH found that the thermal instabilities which they found would continue long enough to increase the burning rate in the shell by a factor of 10 or so. The star would react to the high ϵ by expanding the region outside the shell. But this would cause ϵ to drop to a level commensurate with the new structure of the star, making both the shell and the envelope contract and setting up the thin shell conditions again. Thus the process would occur again and again and could lead to a kind of long term relaxation oscillation. While the timescales involved (of the order of 10^6 years) do not permit the direct observation of this phenomenon in real stars[2], one might be able to deduce its occurence by the presence of stars in anomalous positions on the CMD. Unfortunately the appropriate region for helium-burning shells, the AGB, is not sufficiently populated to offer evidence of this.

What about hydrogen-burning shells? Because of their much smaller dependence of energy generation on temperature, they have not been studied much to this point. But the theoretical discussions do not rule out the possibility that CNO-burning hydrogen shells can be unstable. Most of the models considered by the above authors are post-helium flash, with an inert carbon core and both a helium- and hydrogen-burning shell. The helium-burning shell is at least as significant as the hydrogen-burning shell in energy generation, and so its presence below the latter could add subtle complications to the determination of the instability mechanism. Thus it would be preferable to consider the evolutionary phase after the end of core hydrogen burning when the hydrogen burning shell is well developed, i.e. the RGB, when only a hydrogen shell exists. This lasts 1-5 x 10^8 years for stars with mass $\lesssim$1.2 M$_\odot$, depending on the stellar mass and composition.

In star clusters larger populations of stars exist in this phase, so that the occurence of this instability might produce unusual features on the CMD that are detectable. As mentioned above and shown in Figure 1, NGC 6752 and 288 do display inexplicable gaps in their RGBs. If the gap at V $\sim$ 17.8 is indeed real, it does not seem to be explainable by current standard evolutionary models of stars. These clusters are anomalous in other ways, too: the stars in NGC 6752 exhibit unusual surface abundances[3], and both clusters

have definite, inexplicable gaps in their horizontal branches. Perhaps these traits are in some way connected.

Thus this study was prompted by three factors. First, SH and BE showed that hydrogen-burning shells have some potential for thermal instability. Second, an observational anomaly exists in the CMDs of some globular clusters which may be a clue that thermal instabilities are indeed occurring. And finally, no one has actually applied an instability check to the appropriate stellar models, to confirm or deny their stability.

As an aside, SH also suggested that their technique should be applied to the modelling of stars in all evolutionary phases, to catch other such unexpected instabilities in the future. It is quite possible to miss thermal instabilities if the time step used in the evolving routine is somewhat greater than the e-folding time of the perturbation. They offered considerable caution about concluding that any model is stable without first checking closely. Thus a more mundane goal of this project is to set up a routine that can be added to existing stellar model codes to allow for such a check.

The method used to test stability is essentially identical to that presented by SH modified to allow for oscillatory instability in the manner described by HS. The stars considered are typical of red giants in globular clusters, with masses of 0.8-1.0 $M_\odot$, heavy-element

abundances Z of .0001 to .0169, and helium contents Y of .20 to .30 (where the abundances are given in mass fractions).

Footnotes:

1 - It should be mentioned that there are other forms of instability besides that considered in this paper, such as vibrational instability (see for instance, Kippenhahn and Thomas, 1983). This occurs when volumes of matter rise and fall over ever-greater ranges, as their temperatures over-adjust for convective stability because of the fluctuation of energy generation which accompanies the temperature change.

2 - FG Sagittae is a possible exception to this, it being a peculiar variable star with a period of the order of decades. However, it is not very well understood at present so the occurence of thermal instabilities in it is purely speculative at present. For a recent discussion of this star, see for example Cohen and Phillips (1980).

3 - Freeman and Norris (1981) have written an excellent review of this matter. The cluster NGC 6752 is among many whose stars exhibit large variations in abundances of molecules with C and N. Also noteworthy are a correlation

between CN and both Al and Na and an anticorrelation in the abundances of CN and CH. Neither theories of primordial abundance variations nor atmospheric mixing seem to be able to explain all of these features at present.

2. Theory

Physical properties of stellar interiors

The interior of a star can be described by the following four equations (see for example Schwarzschild 1958, p. 96):

$$\frac{dR}{dM} = \frac{1}{4\pi R^2 D} \tag{3}$$

$$\frac{dP}{dM} = -\frac{GM}{4\pi R^4} \tag{4}$$

$$\frac{dL}{dM} = \epsilon - T\frac{dS}{dt} \tag{5}$$

$$\frac{dT}{dM} = \begin{cases} \dfrac{-3\kappa L}{64\pi^2 acT^3 R^4} & \text{radiative} \\ \left(1-\dfrac{1}{\gamma}\right)\dfrac{T}{P}\dfrac{dP}{dM} & \text{convective} \end{cases} \tag{6}$$

where S is the entropy (dS/dt is quite negligible, except during phases of rapid contraction or expansion). The form of equation (6) depends on the mechanism of energy transport. Generally radiative and convective transport dominate

(conduction is important only in a highly degenerate gas), the prevailing one being determined by the temperature gradient: radiative transport occurs when the absolute magnitude of the gradient is less than the "adiabatic gradient", i.e. when

$$-\left.\frac{dT}{dM}\right|_{adiabat} = (1-\frac{1}{\gamma})\frac{T}{P}\frac{dP}{dM} > -\left.\frac{dT}{dM}\right|_{rad} . \qquad (7)$$

Simple perturbation theory: a) thermal perturbation

Following SH, consider a hydrogen-burning shell of thickness ΔR, containing mass ΔM, and with a temperature drop of $+\Delta T$ (Figure 2). Assume that the rate of change of the entropy in the shell is insignificant. Also assume that the energy transport mechanism is radiation, i.e., the condition defined by equation (7) is fulfilled. And finally assume that the shell is a strong energy source, and that sources below the shell are negligible. Then as the shell and the layers below it are in thermal equilibrium, all of the energy flux goes upwards from the shell, and equation (6) gives

through bottom: $L = 0,$ (8)

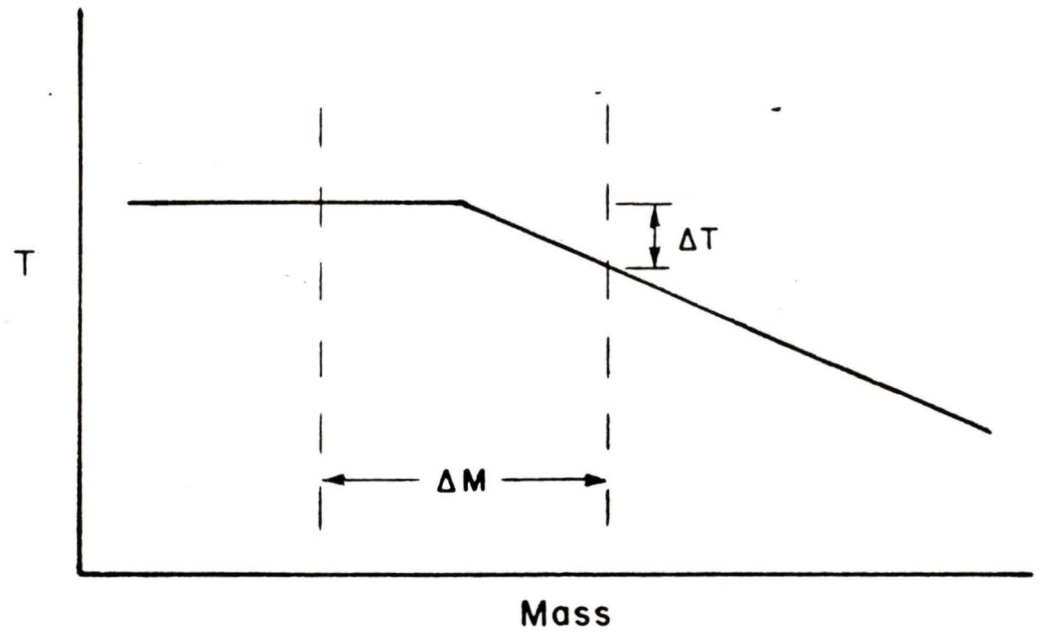

Figure 2: Idealized temperature profile through a nuclear-burning shell (following SH) of width ΔM.

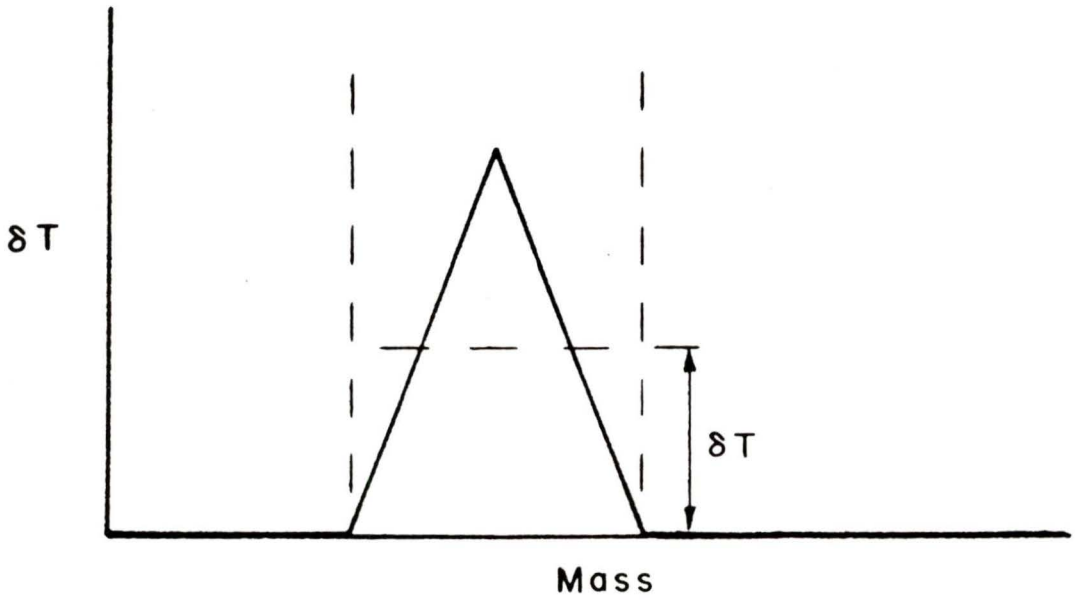

Figure 3: Idealized temperature perturbation through a nuclear-burning shell (following SH) of width ΔM.

through top:
$$L = \frac{64\pi^2 acT^3R^4}{3\kappa} \cdot \frac{\Delta T}{1/2\ \Delta M} \tag{9}$$

Now consider a simple thermal perturbation in the shell, of the form shown in Figure 3. Considering only the significant resulting perturbations, one gets

through bottom:
$$\delta L = -\frac{64\pi^2 acT^3R^4}{3\kappa} \cdot \frac{\Delta T}{1/4\ \Delta M} \tag{10}$$

through top:
$$\delta L = +\frac{64\pi^2 acT^3R^4}{3\kappa} \cdot \frac{\Delta T}{1/4\ \Delta M} \tag{11}$$

Therefore

$$\begin{aligned} \delta\left(\frac{dL}{dM}\right) &= \frac{\delta L(\text{top}) - \delta L(\text{bottom})}{\Delta M} \\ &= \frac{2\ (L(\delta T/\Delta T)*2)}{\Delta M} \\ &= \frac{4L}{\Delta M} \cdot \frac{\delta T}{\Delta T} \\ &= 4 \cdot \frac{L}{\Delta M} \cdot \frac{T}{\Delta T} \cdot \frac{\delta T}{T} \end{aligned} \tag{12}$$

Recalling the temperature dependence of the energy generation from nuclear burning (equation 1) and ignoring perturbations in P and D, then from equation (5):

$$\delta\left(\frac{dL}{dM}\right) = \delta\epsilon - T\frac{d}{dt}(\delta S)$$

or

$$\delta E - \delta\left(\frac{dL}{dM}\right) = -T\frac{d}{dt}(\delta S) \quad .$$

$$\epsilon U \frac{\delta T}{T} - 4 \cdot \frac{L}{\Delta M} \cdot \frac{T}{\Delta T} \cdot \frac{\delta T}{T} = T\frac{d}{dt}(\delta S) \quad . \tag{13}$$

$\epsilon \simeq \Delta L/\Delta M = L/\Delta M$, so

$$\left(U - 4\frac{T}{\Delta T}\right)\frac{L}{\Delta M} \cdot \frac{\delta T}{T} = T\frac{d}{dt}(\delta S)$$

or

$$\left(U - 4\frac{T}{\Delta T}\right)\frac{\delta T}{T} = \left(T\frac{\Delta M}{L}\right) \cdot \frac{d}{dt}(\delta S) \tag{14}$$

The left hand side of equation (14) has 2 terms: the first represents the gain in energy from increasing nuclear burning due to the temperature increase, while the second represents the energy loss due to the resulting increase in radiation. Thus, if the energy gain from increased burning is greater than the increase in the radiative losses, a positive temperature perturbation gives rise to an increase in the entropy in the shell. Consequently one condition for instability is

$$\frac{\Delta T}{T} > \frac{4}{U} \quad . \tag{15}$$

This cannot be met in the case of hydrogen burning by the p-p chain, but is possible by the CNO cycle and for helium burning.

b) hydrostatic readjustment

A second condition is required, to determine whether or not a positive entropy change in turn produces a positive temperature change (in other words, a "thermal runaway" situation).

The readjustment of the structure of a star when the entropy changes is governed by equations (3) and (4). These linearize into

$$\frac{d}{dR}\left(\frac{\delta R}{R}\right) = \frac{1}{R}\left(-3\frac{\delta R}{R} - \frac{\delta D}{D}\right) \qquad (16)$$

and

$$\frac{d}{dR}\left(\frac{\delta P}{P}\right) = \frac{V}{R}\left(4\frac{\delta R}{R} + \frac{\delta P}{P}\right) \qquad (17)$$

where

$$V = -\frac{dP/P}{dR/R} = \frac{D}{P}\cdot\frac{GM}{R} \; . \qquad (18)$$

$\delta D/D$ in (16) can be replaced by using the definition of the entropy

$$T\delta S = \delta U + P\delta(\frac{1}{D}) \tag{19}$$

and the internal kinetic energy for an ideal gas

$$U = \frac{3kT}{2\mu H} = \frac{3}{2}\cdot\frac{P}{D} \tag{20}$$

so that

$$T\delta S = \frac{3}{2}\delta(\frac{P}{D}) + P\delta(\frac{1}{D})$$

$$= \frac{3}{2}\cdot\frac{\delta P}{D} - \frac{3}{2}\cdot\frac{P}{D^2}\delta D - \frac{P}{D^2}\delta D$$

$$= \frac{P}{D}(\frac{3}{2}\cdot\frac{\delta P}{P} - \frac{5}{2}\cdot\frac{\delta D}{D}) \tag{21}$$

or

$$\frac{\delta D}{D} = \frac{3}{5}\cdot\frac{\delta P}{P} - \frac{2}{5}T\frac{D}{P}\delta S \ . \tag{22}$$

Thus equation (16) becomes

$$\frac{d}{dR}(\frac{\delta R}{R}) = \frac{1}{R}\cdot(-3\frac{\delta R}{R} - \frac{3}{5}\cdot\frac{\delta P}{P} + \frac{2}{5}T\frac{D}{P}\delta S) \ . \tag{23}$$

To solve equations (23) and (17) simultaneously, one must use the variations of parameters method with the variables being $\delta R/R$ and $\delta P/P$. This requires two indepen-

dent solutions of the corresponding homogeneous equations (i.e. when $\delta S = 0$), one being regular at each boundary.

Near the centre, equation (18) can be simplified by assuming constant P and D, resulting in

$$V = \frac{Dc^2}{Pc} \cdot \frac{4\pi G}{3} R^2 \quad . \tag{24}$$

Then assuming a form of $a + bV + cV^2 + \ldots$, the first solution expands near the centre as

$$\delta\left(\frac{R}{R}\right)_1 = -\frac{1}{5} - \frac{3}{250}V - \frac{39}{35000}V^2 - \frac{897}{9450000}V^3 - \cdots \tag{25}$$

$$\delta\left(\frac{P}{P}\right)_1 = 1 + \frac{1}{10}V + \frac{13}{1000}V^2 + \frac{299}{210000}V^3 + \cdots \tag{26}$$

Near the surface of the star, where M and L are essentially constant, equations (3), (4), and (6) can be simplified (see for example Schwarzschild 1958, p. 116) to give

$$T = \frac{2}{5}\frac{\mu H}{k} GM\left(\frac{1}{R} - \frac{1}{R_s}\right) \tag{27}$$

if convection is occurring, where R_s is the radius of the star. This together with the equation of state for an ideal gas yields the following simplification of equation (18):

$$\frac{1}{V} = \frac{2}{5}\cdot\left(\frac{Rs-R}{Rs}\right) \quad . \tag{28}$$

If one assumes a form similar to that of the first solution, then the second solution expands near the surface as

$$\left(\frac{\delta R}{R}\right)_2 = -\frac{1}{4} - \frac{3}{20}\left(\frac{Rs-R}{R}\right) - \frac{6}{35}\left(\frac{Rs-R}{R}\right)^2 - \frac{4}{21}\left(\frac{Rs-R}{R}\right)^3 - \cdots \tag{29}$$

$$\left(\frac{\delta P}{P}\right)_2 = 1 + \frac{3}{7}\left(\frac{Rs-R}{R}\right) + \frac{10}{21}\left(\frac{Rs-R}{R}\right)^2 + \frac{40}{77}\left(\frac{Rs-R}{R}\right)^3 + \cdots \tag{30}$$

Given these two solutions, the variation of parameters method may be employed (see for example Boyce and DiPrima, 1977). Rewrite (23) and (17) as

$$\frac{d\bar{x}}{dR} = P(R)\cdot\bar{x} + \bar{g}(R) \tag{31}$$

where

$$P(R) = \begin{pmatrix} -\frac{3}{R} & -\frac{3}{5R} \\ 4\frac{V}{R} & \frac{V}{R} \end{pmatrix} \tag{32}$$

and

$$\bar{x} = \begin{pmatrix} \frac{\delta R}{R} \\ \frac{\delta P}{P} \end{pmatrix}, \qquad \bar{g}(R) = \begin{pmatrix} \frac{2}{5}T\frac{D}{P}\cdot\frac{\delta S}{R} \\ 0 \end{pmatrix} \quad . \tag{33}$$

Then if

$$Y(R) = \begin{pmatrix} (\frac{\delta R}{R})_1 & (\frac{\delta R}{R})_2 \\ (\frac{\delta P}{P})_1 & (\frac{\delta P}{P})_2 \end{pmatrix} . \qquad (34)$$

is the fundamental solution of

$$\frac{d\bar{x}}{dR} = P(R) \cdot \bar{x} \ , \qquad (35)$$

the solution to (31) is given by

$$\bar{x} = Y(R) \cdot c + Y(R) \int_{Ro}^{R} Y^{-1}(s) \bar{g}(s) ds \ . \qquad (36)$$

where c is an arbitrary constant.

Y^{-1} is easily obtained as Y is only a 2 x 2 matrix:

$$Y^{-1}(R) = \begin{pmatrix} -(\frac{\delta P}{P})_2 & (\frac{\delta R}{R})_2 \\ (\frac{\delta P}{P})_1 & -(\frac{\delta R}{R})_1 \end{pmatrix} \cdot \frac{1}{((\frac{\delta R}{R})_2 (\frac{\delta P}{P})_1 - (\frac{\delta P}{P})_2 (\frac{\delta R}{R})_1)} . \qquad (37)$$

If c is set to zero, this leads to

$$\frac{\delta R}{R} = (\frac{\delta R}{R})_1 \int_{R}^{Rs} \frac{Q}{(\delta P/P)_1} \cdot \frac{2}{5} T \frac{D}{P} \delta S \frac{\delta R}{R} + (\frac{\delta R}{R})_2 \int_{0}^{R} \frac{Q}{(\delta P/P)_2} \cdot \frac{2}{5} T \frac{D}{P} \delta S \frac{\delta R}{R} \qquad (38)$$

$$\frac{\delta P}{P} = \left(\frac{\delta P}{P}\right)_1 \int_R^{Rs} \frac{Q}{(\delta P/P)_1} \cdot \frac{2}{5} T \frac{D}{P} \delta S \frac{\delta R}{R} \; + \; \left(\frac{\delta P}{P}\right)_2 \int_0^R \frac{Q}{(\delta P/P)_2} \cdot \frac{2}{5} T \frac{D}{P} \delta S \frac{\delta R}{R} \qquad (39)$$

with

$$Q = \left(\frac{(\delta R/R)_2}{(\delta P/P)_2} - \frac{(\delta R/R)_1}{(\delta P/P)_1} \right)^{-1} . \qquad (40)$$

Equation (39) can be crudely simplified to

$$\frac{\delta P}{P} = \frac{2}{5} Q \frac{\Delta R}{R} \cdot T \frac{D}{P} \delta S \qquad (41)$$

for the case where the entropy perturbation δS is occurring in a thin shell. Q is not a constant, but does vary smoothly over the relatively small range of -8 to -4 for nearly all of the star. Thus this equation shows that a positive entropy perturbation leads to a negative pressure perturbation, as expected. However, this is not necessarily true for the temperature perturbation. Using the ideal gas law, equation (41) becomes

$$\frac{\delta T}{T} = \frac{2}{5} \left(1 + \frac{2}{5} Q \frac{\Delta R}{R}\right) T \frac{D}{p} \delta S \; . \qquad (42)$$

Clearly the temperature perturbation is going to be <u>positive</u> if the shell is very thin, i.e.

$$\frac{\Delta R}{R} < \frac{5}{2} \frac{1}{|Q|} \cdot \qquad (43)$$

So if this condition and that given by equation (15) are met, the shell should be thermally unstable. Both conditions are rather crude, but they certainly should delineate roughly any regions of interest.

One last simplification that can be made comes from the observation of the models that the relative temperature drop ($\Delta T/T$) is roughly two thirds that of the relative thickness ($\Delta R/R$) of well-developed shells. Using a median value of -6 for Q, the two conditions may be satisfied simultaneously if

$$U \gtrsim 15 \, . \qquad (44)$$

Thus helium-burning and CNO hydrogen-burning shells must certainly be considered for potential instabilities.

3. Computational Technique

To properly study thermal stability one must first create an accurate model of the desired star. The standard way is to use the Henyey scheme on an initial guess of the stellar structure, and iteratively converge the model until equations (3) to (6) are satisfied. A simple explanation of this technique follows; for a more detailed description, see Henyey et al. (1964).

The stellar model is assumed to consist of a large number (typically 100 to 400) of spherically concentric shells. The total mass contained within the outer boundary of each shell is taken to be the independent variable, thus defining the shells. The four dependent variables - radius, luminosity, pressure, and temperature - are then expressed as functions of the mass. The desired goal is to have all four of the stellar structure equations satisfied at every point throughout the star, to within some stringent criterion.

Assuming that enough layers exist such that the change in the dependent variables from one grid point to the next is approximately linear, the differential equations typified by

$$\frac{du}{dM} = f(u,v,w,x,M) \tag{45}$$

may be approximated by difference equations expressed as

$$F = \frac{u_{i+1} - u_i}{M_{i+1} - M_i} - \frac{f_{i+1} + f_i}{2} = 0 \ . \tag{46}$$

Now, modifying Newton's method of solving a single equation with one unknown, one can write

$$0 = F(u_i + \delta u_i, u_{i+1} + \delta u_{i+1}, v_i + \delta v_i, \ldots) =$$

$$F(u_i, u_{i+1}, v_i, \ldots) + \frac{dF}{du_i}\delta u_i + \frac{dF}{du_{i+1}}\delta u_{i+1} + \frac{dF}{dv_i}\delta v_i + \ldots \tag{47}$$

where the δ's are the corrections to be applied to the variables u, v, w, and x. This can be written for each of the four equations for each of the n-1 layers between the first and nth grid points, thus giving 4(n-1) equations in 4n unknowns (the corrections).

Four more equations are needed. These come from the boundaries of the star, the centre and surface. In place of the usual two central boundary conditions (L = 0 and M = 0 at R = 0, which would be problematic as most variables are expressed in the computer code in logarithmic form), approximations to equations (3) and (5) are adopted instead:

$$M = \frac{4}{3}\pi R^3 D \tag{48}$$

and

$$L = \epsilon M \ . \tag{49}$$

This assumes that the innermost grid point is sufficiently close to the centre that D, T, the composition, and dS/dt are constant over the region inside the shell.

For the surface zone, it is best to separately model the stellar atmosphere and consider the first layer to be considered in the Henyey code to be somewhat below the actual surface (typically at the point where the mass is .99 that of the total). This is primarily to isolate the steep changes in variables such as P over a very small change in mass that occur in the outer region.

The "surface" of a star is defined as the point where the actual temperature equals the effective temperature Te of the star (the temperature of a black body that produces a radiation spectrum similar to that of the star). Assuming a Gray atmosphere approximation[1], the two temperatures are related in the following manner:

$$T^4 = \frac{3}{4}Te^4(\tau + \frac{2}{3}) \tag{50}$$

where τ, the optical depth, is defined from

$$d\tau = -\kappa D dR \ , \qquad (51)$$

and κ is the mean absorption coefficient. At this "surface" (the photosphere), where $\tau = 2/3$, the luminosity and radius of the star are related by

$$L = 4\pi\sigma R^2 Te^4 \ . \qquad (52)$$

On the assumption that the position of the model on the CMD is known, L and Te are then defined. R can be obtained from equation (52), so only the photospheric pressure P remains to be determined. Using equations (3), (4), and (51), P and the optical depth are related by

$$\frac{dP}{d\tau} = \frac{GM}{\kappa R^2} = \frac{g}{\kappa} \ , \qquad (53)$$

where g is the gravitational acceleration which is effectively constant throughout the atmosphere. This can be used to determine P at $\tau = 2/3$ to a reasonable degree of accuracy by a numerical integration where τ is incremented from a very small number, say 0.0001, to 2/3. This must be done in conjunction with equation (50), however, as κ is a function of both T and P.

Given these four values at $\tau = 2/3$, equations (3) to (6) can be integrated via the Runge-Kutta method down to the point where the mass is .99 that of the total, which is the

first grid point of the main stellar model. Equation (5) can be eliminated since the luminosity is a constant throughout this entire surface layer, thereby simplifying the procedure.

All of this assumes that it is known precisely where on the CMD the model resides. As this isn't the case, the triangle strategy of Kippenhahn, Weigert, and Hofmeister (1967) is employed. Three model atmospheres are computed at points on the CMD that form a right triangle around the region where the model is estimated to reside. It is then assumed that over the entire region enclosed by the triangle

$$R = aP^{b}T^{c} \tag{54}$$

and

$$L = dP^{e}T^{f} \text{ ,} \tag{55}$$

where a, b, c, d, e, and f are constants which must be determined. If the triangle is small enough, this is a good approximation. As R, L, P, and T are all known at the bottom of the three atmospheres, six equations are available to solve for the six constants, a to f. Therefore two boundary conditions exist for any model that falls within the triangle[2]:

$$R = f(P,T) \tag{56}$$

and

$$L = f(P,T) \ . \qquad (57)$$

With these four boundary equations - (48), (49), (56), and (57) - expressed as difference equations, 4n equations in 4n unknowns are obtained. This system is solvable by simply triangularizing the matrix of coefficients and then back substituting to obtain δu, δv, δw, and δx for each layer. These corrections are then applied to the current model, and the process is repeated until all the corrections drop to less than some chosen criterion of accuracy.

Given a converged model, one can also simulate evolution by converting an amount of fuel to the appropriate products (as dictated by the time step chosen and the fusion rate specified by the model) and reconverging this slightly different model. Thus one can create a stellar model of any desired age.

Many refinements can be introduced to the simple procedure outlined above to improve the accuracy of the model, so as to achieve good agreement with observations. For example, the number of shells describing the star can be increased between evolutionary steps so as to minimize the change in the dependent variables or composition between layers, the energy loss due to neutrinos and/or other products of exotic fusion processes can be incorporated, and more realistic model atmospheres can be adopted as boundary conditions. Some of the most accurate models to date are

those by VandenBerg (1983), and the same modelling program has been used in this study.

The Stability Test

Having created a model of the star and evolved it to the desired age, the stability test mechanism can be introduced. Again the four basic equations must be considered simultaneously. Assume that a perturbation of the star occurs, and that the time variation of all perturbations follow a simple exponential:

$$\delta L,\ \delta R,\ \delta P,\ \delta T \ \propto\ e^{+t/\tau} \qquad (58)$$

where t is the time and τ is the eigenparameter[3] (which is, in general, assumed to be complex). A positive real component of τ means the perturbation would grow (and thus would be unstable), a negative real component means the perturbation would be damped out, and an imaginary component of either sign means an oscillatory component would exist. Possible resultant perturbations in chemical composition due to the change in energy generation rate are ignored, on the assumption that they are minor (composition changes are very slow and smooth).

The four main equations become:

$$\delta\left(\frac{dR}{dM}\right) = \frac{1}{4\pi}\delta\left(\frac{1}{R^2 D}\right) \tag{59}$$

$$\delta\left(\frac{dP}{dM}\right) = \frac{G}{4\pi}\delta\left(\frac{M}{R^4}\right) \tag{60}$$

$$\delta\left(\frac{dL}{dM}\right) = \delta\epsilon - \delta(T)\cdot\frac{dS}{dt} + T\frac{\delta(S)}{\tau} \tag{61}$$

$$\delta\left(\frac{dT}{dM}\right) = \begin{cases} \dfrac{-3\kappa}{64\pi^2 ac}\,\delta\left(\dfrac{L}{T^3 R^4}\right) & \text{radiative} \\ \left(1-\dfrac{1}{\gamma}\right)\delta\left(\dfrac{T}{P}\cdot\dfrac{dP}{dM}\right) & \text{convective} . \end{cases} \tag{62}$$

As the primary variables are known at every point in the star, the four perturbations at each level are the only unknowns.

Note that equation (61) has an explicit time derivative and thus has a new term in it. This is the only place where τ appears explicitly. When these equations are replaced by the appropriate difference equations, the only change from those used to converge the model is due to this last term. This is convenient as the same computer code may then be used, if one simply adds in the appropriate set of coefficients involving τ where needed (see Appendix I for a

listing and documentation of the code used to obtain the eigenparameter).

The difference equations with the 4 boundary equations form a set of linear, homogeneous equations just equal to the number of unknown perturbation values. It is a four dimensional first-order eigenvalue problem with the reciprocal of the e-folding time, $1/\tau$, as the eigenparameter. To get a non-trivial solution, the determinant of the matrix of the set of coefficients must be zero. The determinant is calculated by triangularizing the matrix and multiplying the diagonal elements together. Most of the numerical work therefore consists of computing the determinant for many trial values of the eigenparameter over a wide range, to find the most significant zeros (usually those having the largest inverse of the real component).

This is a tedious procedure, especially as one is dealing with complex numbers, thus requiring a two-dimensional plane of values of τ. A further complication is that the determinant cannot be handled by most computing languages in a straightforward manner, as it is too large to store in exponential form and logarithms of complex numbers are usually not allowed. The solution to this problem is to express the determinant in polar form, i.e.

$$D = X \cdot e^{iY} \tag{63}$$

where X = |D| and Y = $\tan^{-1}$ ((imaginary part of D)/(real part of D)). X can be expressed in logarithmic form as it is real and Y lies between 0 and 2π, and they uniquely describe D. In practice, only the angle Y is used to find zeros, by noting where it is a multiple of $\pi/2$, so only one small real number need be stored.

Another detail that should be mentioned at this point is that the time step Δt used in this procedure should be kept significantly smaller than the time step used to evolve the models. This is because the eigenparameter is much more sensitive to the change in time of S than the star as a whole is. In practice, this means that if the evolutionary timestep being used near the base of the RGB is, say, 3 x 10^6 years, one should use a time step of only 10^3 to 10^4 years to calculate τ.

Fortunately, the resulting values of the determinant form predictable patterns in the plane of the eigenparameter so that shortcuts do exist (see the following section for examples). Using a VAX 750 computer each trial takes about 0.2 seconds, and a typical simple run, when one knows the general regions of interest, takes about 1 1/2 to 2 hours of CPU time. On an IBM 3083, the time is reduced by a factor of roughly 30.

Once an eigenparameter has been found, additional information may be obtained by looking at its associated eigensolution. This is the vector solution $\bar{x}$ to the

equation

$$D\bar{x} = \bar{0} \qquad (64)$$

where D is the matrix of coefficients involving the eigen-parameter. As the determinant of the matrix is zero, the last diagonal element of the determinant when it has been triangularized is zero. This results in the last element of the solution vector of perturbations being arbitrary and all of the others being scaled to it. This vector shows how the layers of the star react to the perturbation.

Footnotes:

1 - A Gray atmosphere is one for which it is assumed that κ, the mean absorption coefficient, is independent of the frequency - see for example Novotny (1973).

2 - A major benefit of the triangle strategy is that it greatly minimizes the number of times that an atmosphere need be calculated. Three atmospheres suffice for all models within the triangle, and when the evolutionary

sequence moves out of the triangle, two of the atmospheres can be reused as vertices in the new triangle created.

3 - The terms "eigenparameter" and "eigensolution" are used throughout this study to denote, respectively, the parameter y and its associated vector $\overline{x}$ that satisfy the following equation:

$$D(y)\cdot\overline{x} = \overline{0}$$

where D is an array of coefficients that are functions of y. $\overline{x}$ can be non-zero only when the determinant of D is equal to zero, which in general only occurs for a few specific values of y. This definition does not agree strictly with the usual mathematical definition of eigenelements; however, it has been adopted in the literature (i.e. see SH) and thus is used here.

4. Results

The stability test has been applied to six model evolutionary sequences at various points from just before the turnoff point to roughly half way up the RGB. They were chosen to reflect a range of Y, Z and mass reasonably typical for globular cluster red giants, and to allow the determination of the significance of each parameter. One star has been followed to within 10^5 years of the helium flash point, to verify the stability test on that known instability (as SH did). Table 1 gives some of the main characteristics of the models studied.

Figure 4 is a sample "determinant map" created from a grid of trial values of τ. The curves show where the components of the determinant are equal to zero, obtained by connecting points of sign change. Where they cross is a true zero or eigenparameter, as both components are equal to zero. Zeros seem to occur only in two formats, that of a real zero line crossing the real axis (which is an imaginary zero line), and that where the real and imaginary lines double back as seen in the central part of the Figure. This is fortunate, as a grid search pattern can be designed to catch just these features.

Figures 4 and 5 show the evolution of the determinant map for star R1, and Figure 6 shows where these models lie

Table 1: Main characteristics of six model stars

Star	Mass ($M_\odot$)	Xo	Yo	Zo	Age at He Flash (10^9 yrs)	Range in Age of Models (10^9 yrs)
R1	0.8	0.7999	0.2	0.0001	18.3631	1.14-18.3630
R2	0.8	0.799	0.2	0.001	20.057	1.05-20.041
R3	0.9	0.799	0.2	0.001	13.043	0.84-13.031
R4	0.9	0.794	0.2	0.006	18.588	1.21-18.553
R5	0.8	0.699	0.3	0.001	10.769	0.82-10.759
R9	0.9	0.7331	0.25	0.0169	20.87	1.57-20.569

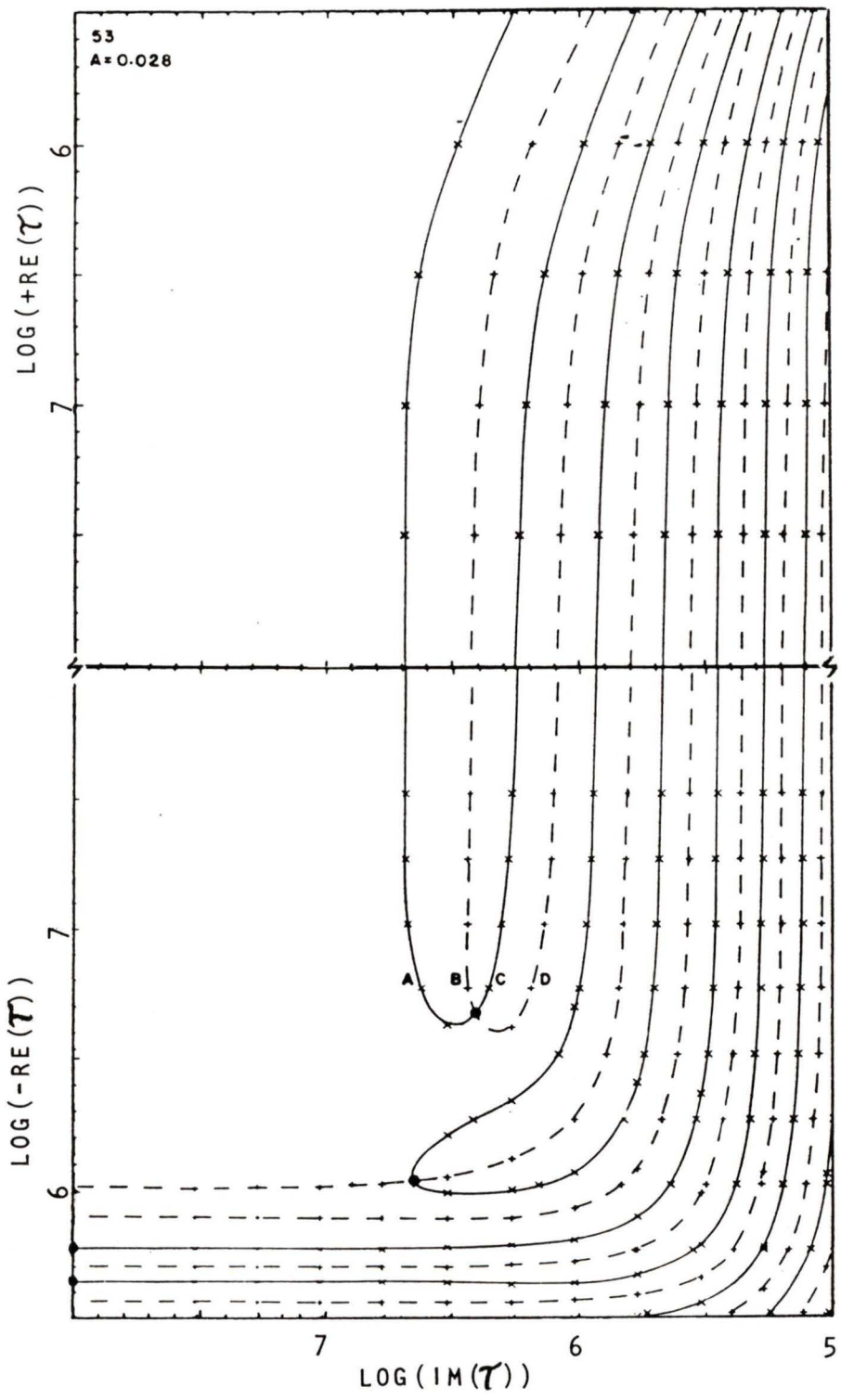

Figure 4: Sample determinant map: model 53 of star R1 (A=0.028). Solid curves are zeros of the real part of the determinant, dashed curves are those of the imaginary part. Where they cross (heavy dots) are zeros of the determinant. The left side of real axis is a mirror image of the right side. τ is in years.

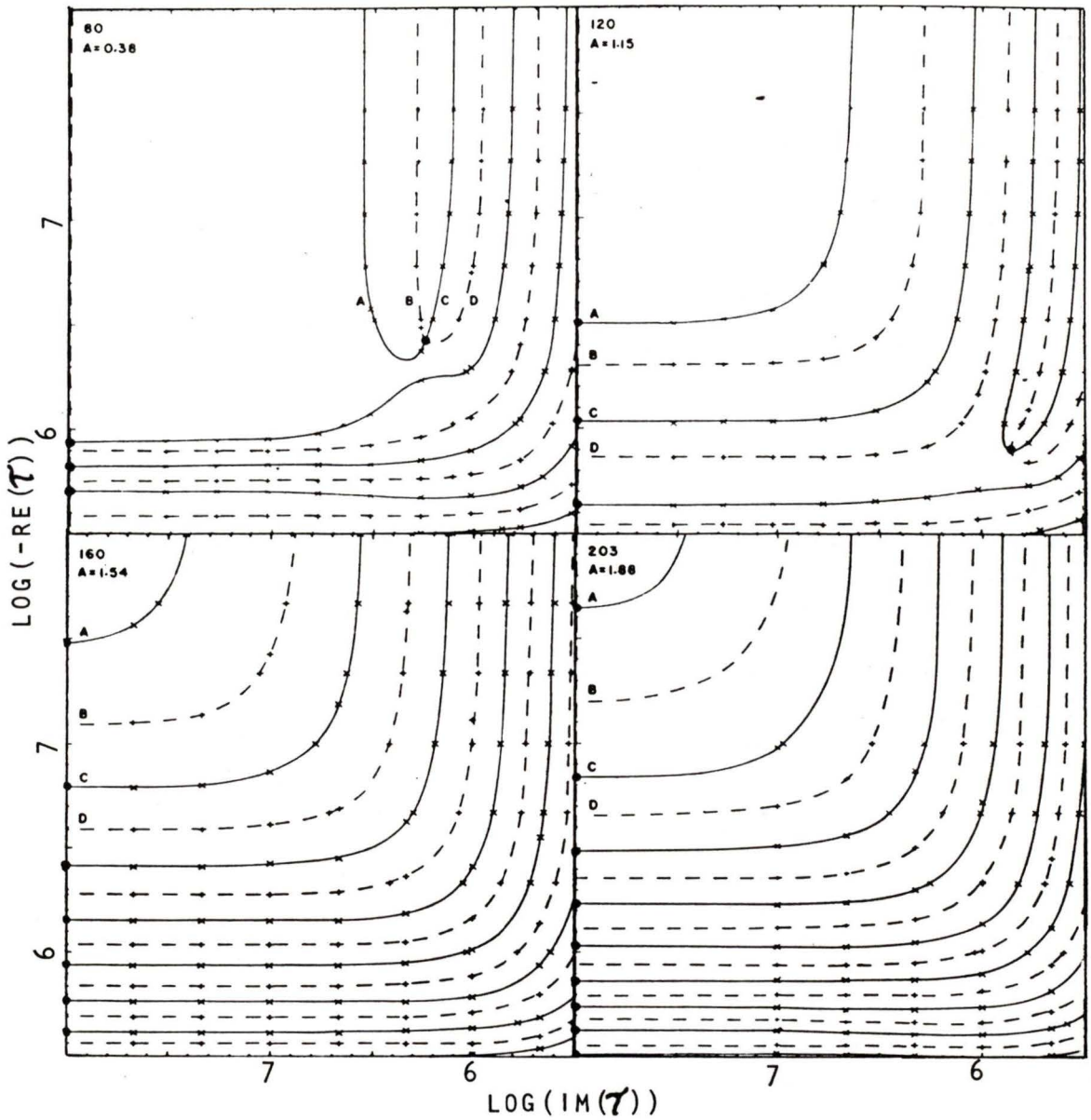

Figure 5: Determinant maps for R1 at seven different ages. See also Figure 4 for model 53. Solid curves are zeros of the real part of the determinant, dashed curves are those of the imaginary part. Heavy dots are eigenparameters. τ is in years. Continued on next page.

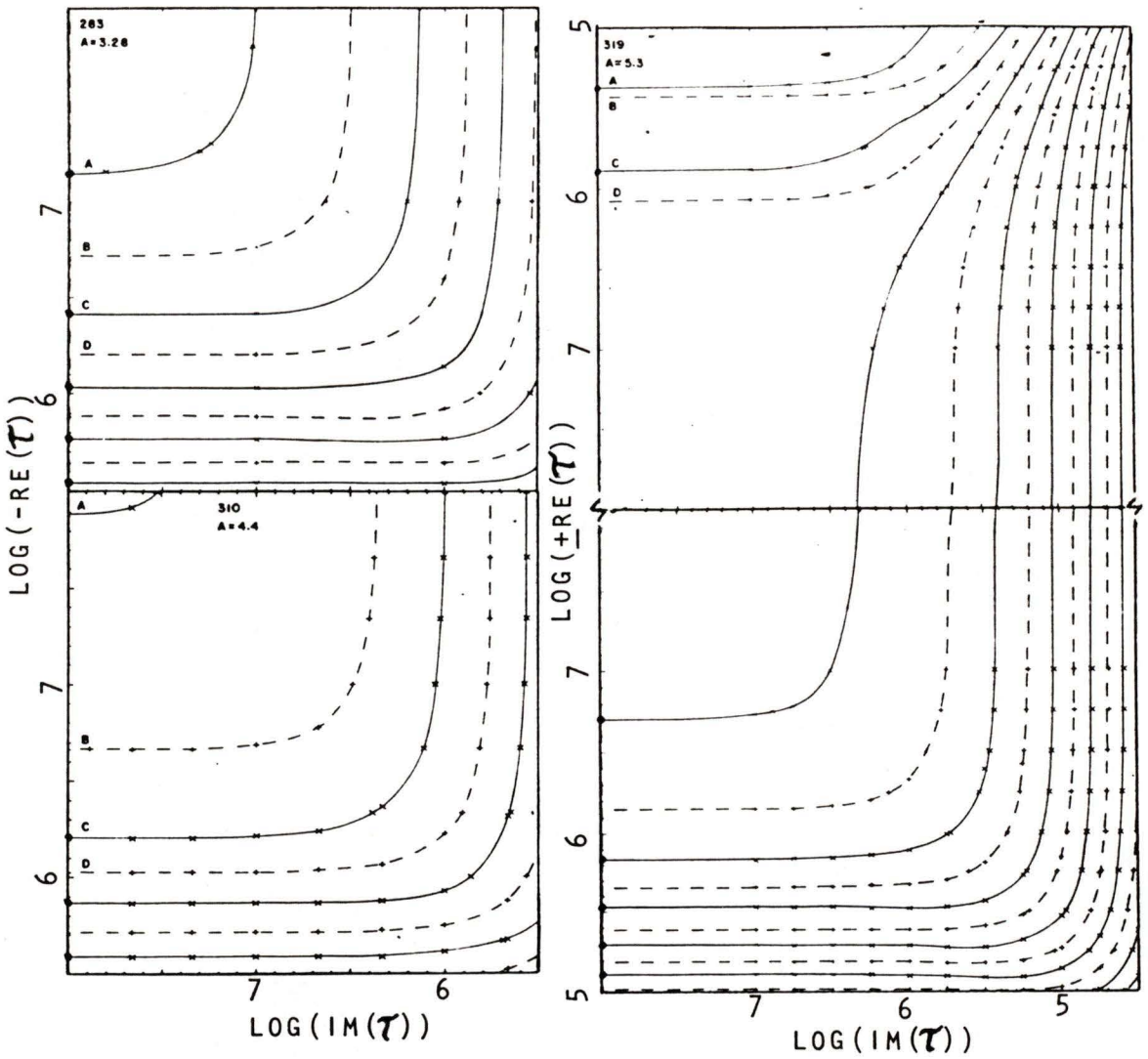

Figure 5: Continued.

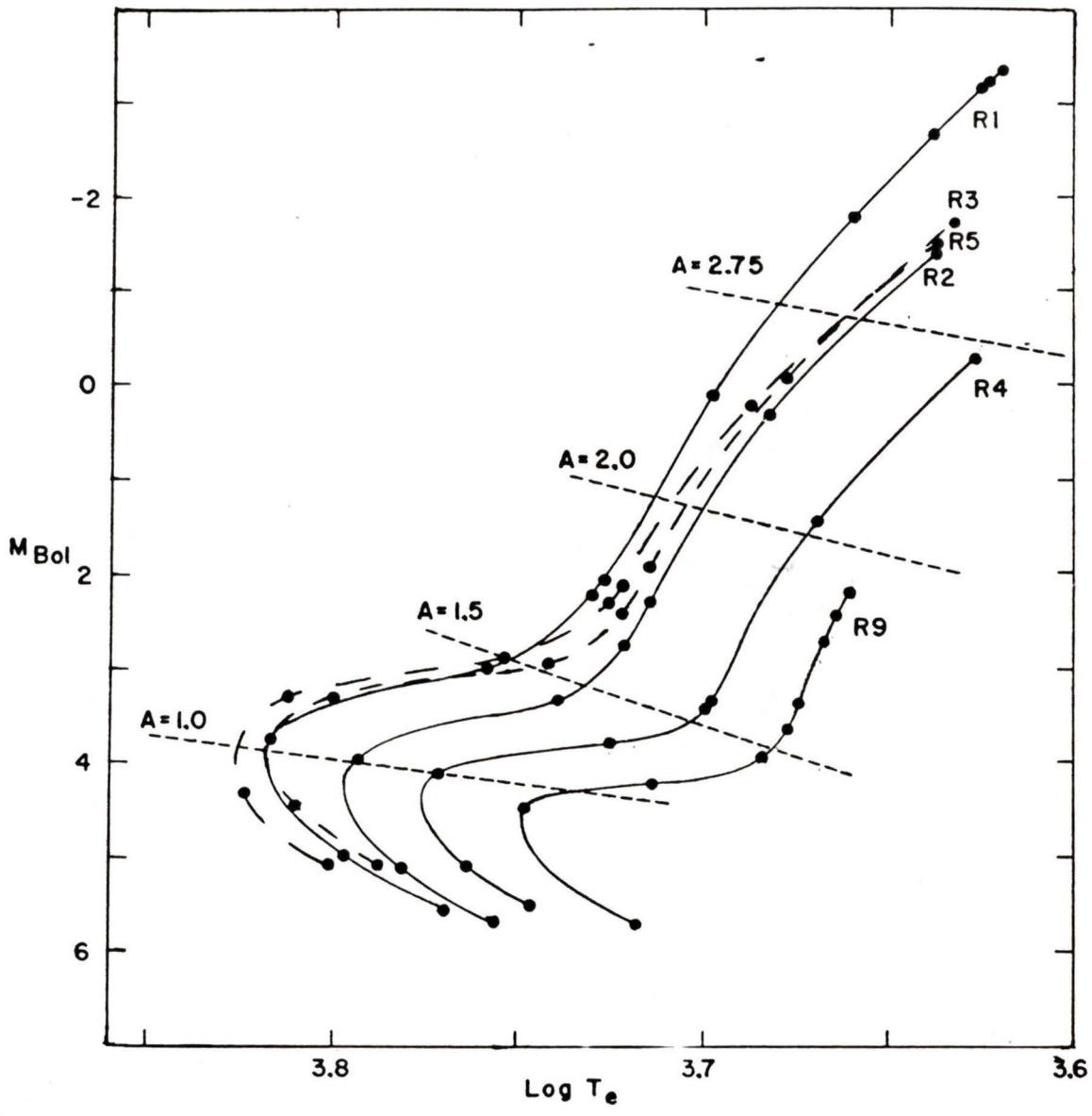

Figure 6: Hertzsprung-Russell Diagram showing evolutionary tracks for 6 model stars. See Table 1 for main characteristics of the models, and text for definition of A. Te is the effective surface temperature. Bolemetric corrections must be applied to M_{Bol} to give M_V. Figure 6 is the theoretical counterpart to Figure 1.

on the CMD. All six models show a similar progession. The first interesting point to note is how the complex zeros (those off of the real axis) drift off to insignificance once the hydrogen shell forms. This contrasts with the results for helium-burning shells obtained by others, where the complex zeros play an important role. HS deduced from studying the eigensolutions that the helium shell is a driving region and a layer below it is a reacting region, reacting to the perturbation out of phase and thus generating an oscillation. Consequently the insignificance of complex zeros implies that for a hydrogen-burning shell there is no reacting region: it operates alone.

The second point of interest is the movement of the first zero, or largest value of $1/\tau$. Clearly this zero is the most important as it would be the first to cross into the unstable half of the plane (assuming, as seems to be the case, that the complex zeros remain in the stable half). Figures 7a and 7b plot the evolution of this zero for the six stars as well as two secondary zeros for R1. The independent variable chosen is

$$A = \text{Log}\left(\frac{\text{Age at helium flash}}{\text{Age at helium flash} - \text{Age}}\right) \qquad (65)$$

as this takes into account the different evolutionary rates of the stars. The position of the hydrogen shell, in terms of the mass it encloses, would also be a good variable to

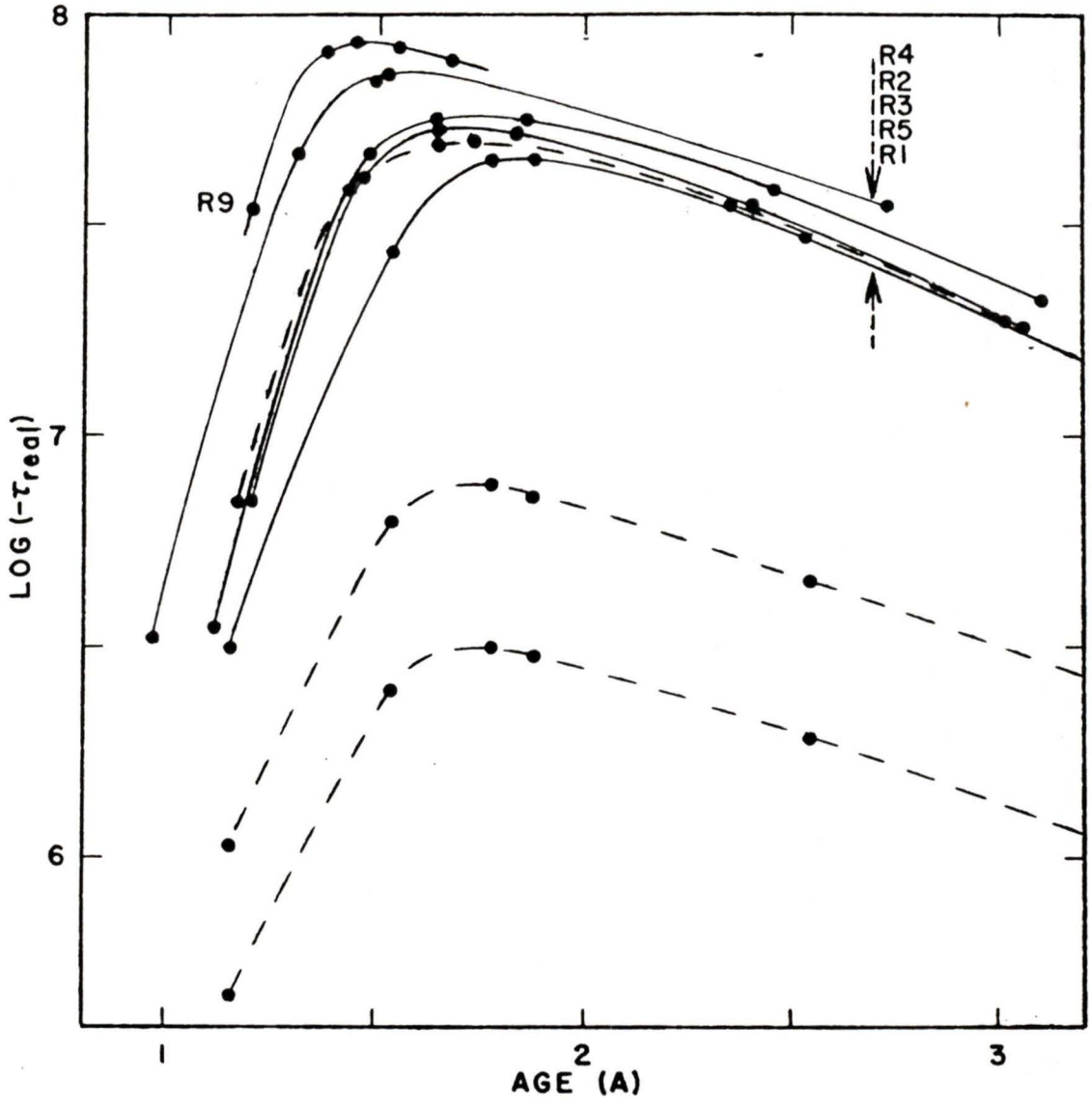

Figure 7a: Evolution of most significant eigenparameter for 6 model stars. Also shown are two secondary eigenparameters for R1. τ is in years.

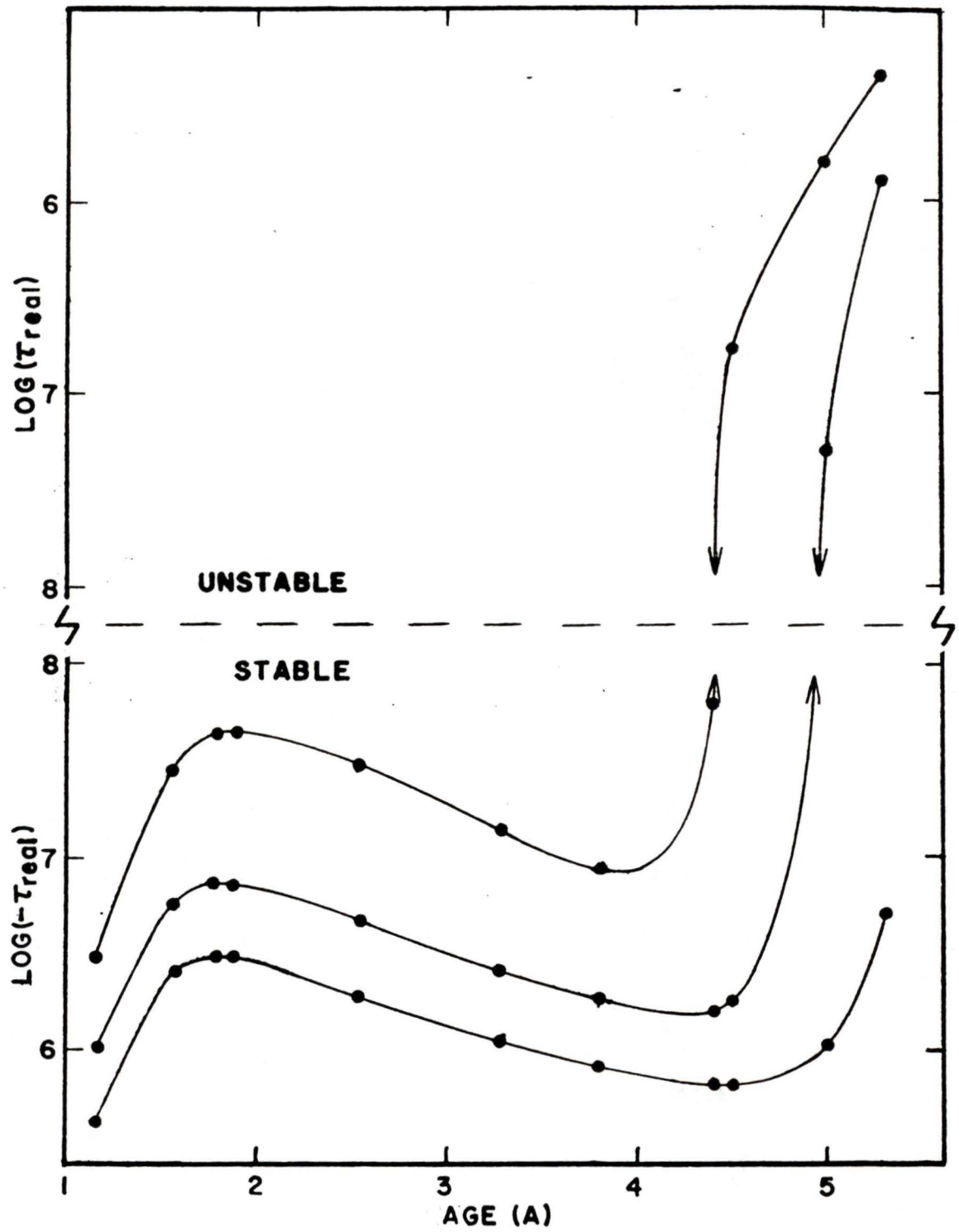

Figure 7b: Evolution of three most significant eigenparameters for R1. τ is in years.

use: Figure 8 shows how the two relate. Prominently exhibited is a local maximum at the point when the stars are at or just past the base of the RGB (see Figure 6): this indicates that the star is tending towards instability as it gets to the base, and then backs off as it proceeds up the RGB (only to reverse direction and become unstable near the tip where the helium flash occurs). Note also how the secondary zeros of R1 follow the curve, but are displaced downwards by a fairly constant amount.

Referring to Figure 6 and Table 1, it is clear that metallicity (i.e. heavy element content) changes have the largest effects. Increasing Z by an order of magnitude increases τ by roughly .15 in the log, or 40%. Table 2 summarizes the effects of changing each parameter as derived from the Figure.

For none of the 6 normal models studied did this maximum actually cross into the unstable half of the plane. But observations of how R1 crossed into the half later on indicate that R9 may be very close. It is thus tempting to simply chose a model similar to R9 but of less mass and Y and greater Z, in an attempt to force a model to go unstable. Unfortunately, these parameters also effect the lifespan of the star, and would do so all in the same direction; upwards. As globular clusters seem to be about 15×10^9 years old, the models should be kept to no more than that to be realistic. As is, R9 is already somewhat

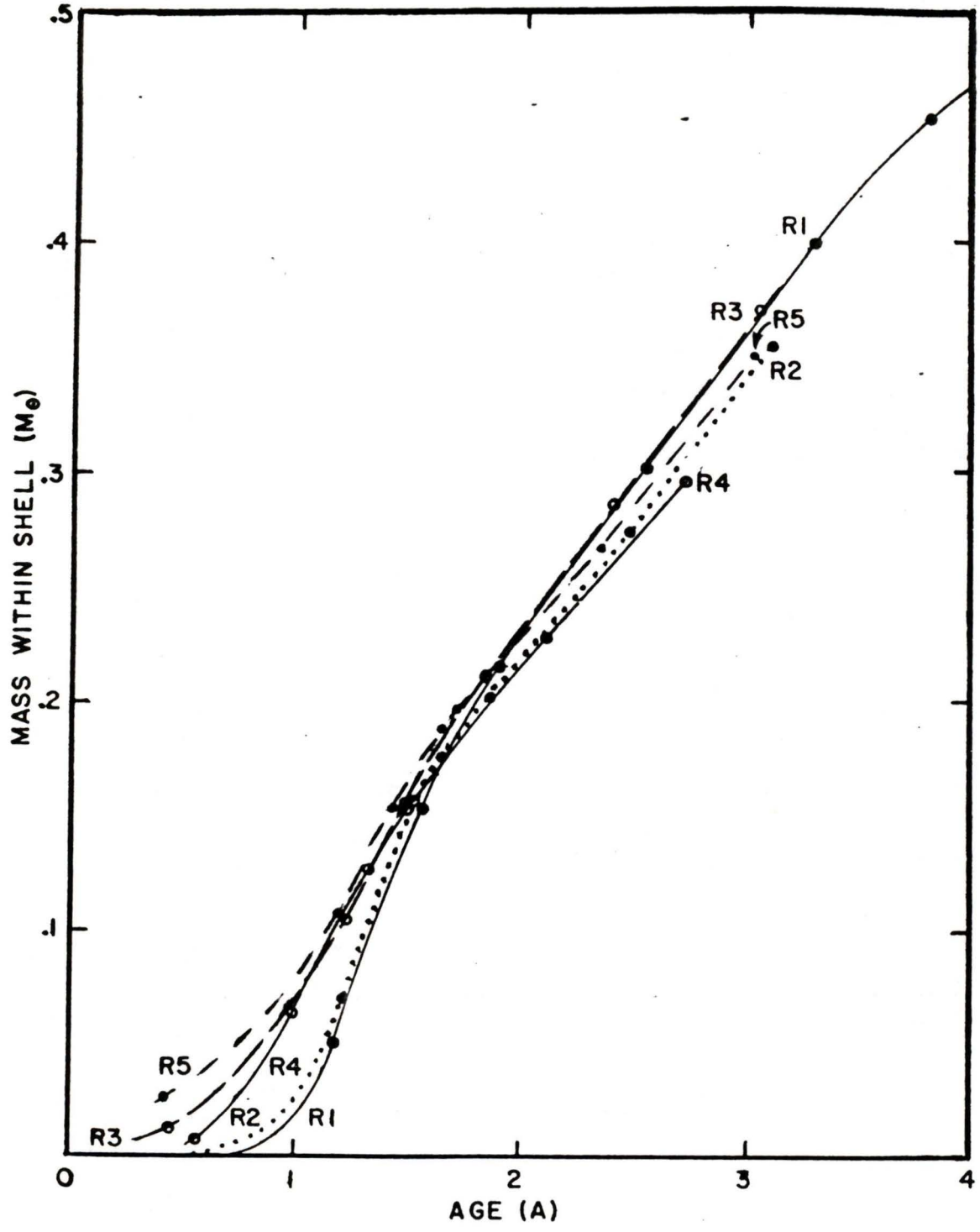

Figure 8: Mass enclosed by shell versus age.

Table 2: Influence of Parameters on τ

Parameter	Range Considered	$\Delta\tau$	Importance
Mass	0.8 - 0.9 $M_\odot$	-10 %	3
Yo	0.2 - 0.3	-15 %	2
Zo	0.0001 - 0.0169	+100 %	1

unrealistic, having an age of 20 x 10^9 years at the base of the RGB.

How do these results compare to the conditions for instability derived in Chapter 2? It is surprising in light of equation (44) that none of the stars ever become unstable. A more detailed examination of the conditions is required.

The crude conditions given by equations (15) and (43) may be applied to the models to determine where instability is predicted. Shell thickness is the heart of the conditions, and its evolution is shown in Figure 9. By A $\simeq$ 1.8 the shell thickness has stabilized in terms of both $\Delta T/T$ and $\Delta R/R$, so that the only change from that point onwards is due to U. R9 and R4, the least stable stellar models, have the thinnest shells when the maximum τ occurs, even though that point occurs earlier for them than for the other stars. Referring to the two equations, this means that for them the temperature condition is harder to satisfy while the radial thickness condition is easier. This tends to push the region where satisfaction of the conditions could overlap to an earlier time for the less stable stars, which agrees with what is observed in Figure 7.

Figure 10 plots the conditions for R4 (using two different definitions of the shell's boundary). The temperature drop condition is satisfied until about the base of the RGB, while the radial thickness condition is

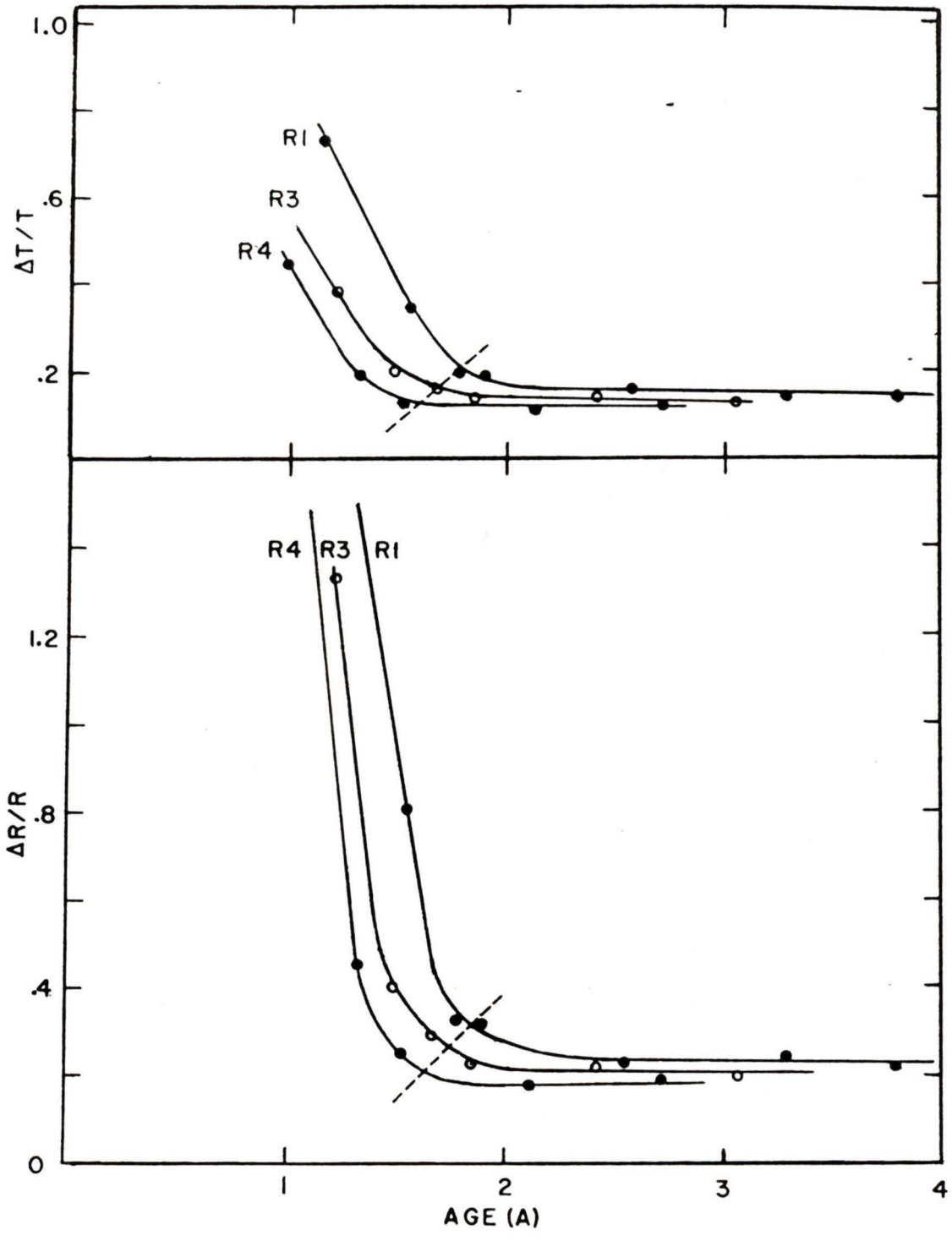

Figure 9: Shell thickness in terms of temperature drop and radial thickness versus age for three model stars. Dashed line indicates where the point of least stability occurs.

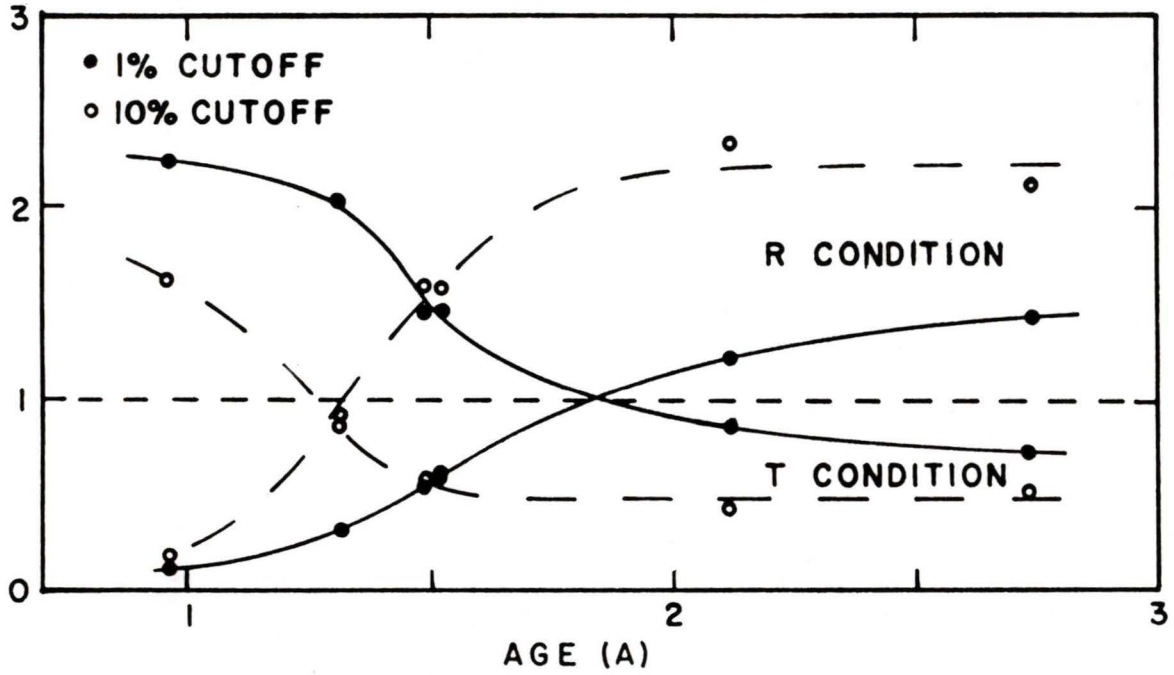

Figure 10: Conditions for instability versus age for R4. Conditions defined by equations (15) and (43) are satisfied if greater than 1.0.

satisfied only going up the RGB. Thus the only region where both could be satisfied is near the base of the RGB. Some overlap exists in the Figure, but the approximations made in the derivation of the conditions and the difficulty in determining Q accurately probably introduce uncertainties of a few tens of percent in each locus. Raising or lowering either curve by even 20% would dramatically alter the amount of overlap. Also, the definition of the shell boundary, which is important in determining ΔT and ΔR, is somewhat arbitrary. Changing it to where the energy generation drops to 10% instead of 1% moves the overlap region for all stars to the left by 0.4 - 0.6 in A. However, the diagram is precise enough to show that the region of least stability occurs in the neighborhood of the base of the RGB and that τ peaks earlier for the least stable stars.

Reasonably good agreement therefore exists between the theoretical conditions and the results of the detailed determinant map calculations. However, more information as to what is happening in the shell as it evolves is necessary to better understand the true nature of the instability phenomenon. In particular, it is not known just how close any of the stars come to becoming unstable, and thus whether or not it can occur at all.

a) Structure of the shell with time

The shell has been defined as the region of greatest nuclear burning. Specifically, the point of maximum nuclear energy generation is taken as the centre and where it falls to 1% as the edge. Figure 11 shows the evolution of the energy generation profile of the shell with time.

The temperature in the shell steadily increases with time, while both the density and pressure peak shortly before the base of the RGB - see Figure 12. ψ, a measure of the electron degeneracy, is also shown. While true degeneracy is never achieved in the shell, a definite maximum occurs at A $\simeq$ 1.2. This Figure shows that the shell undergoes maximum compression shortly before the base of the RGB. What is interesting although unexpected is that the least stable stars are subjected to the least compression and degeneracy. It is not clear why this would be so.

The temperature dependence of the energy generation, υ, also peaks at about A = 1.0 - 1.3. Figure 13 shows this: the most metal rich stars precede in time and excel in magnitude, in a manner quite reminiscent of τ in Figure 7. The different levels of υ between stars and the falloff of υ after the peak is almost certainly due to the difference in the temperature in the shell between models. Equation (1) is only a first order approximation of the relationship

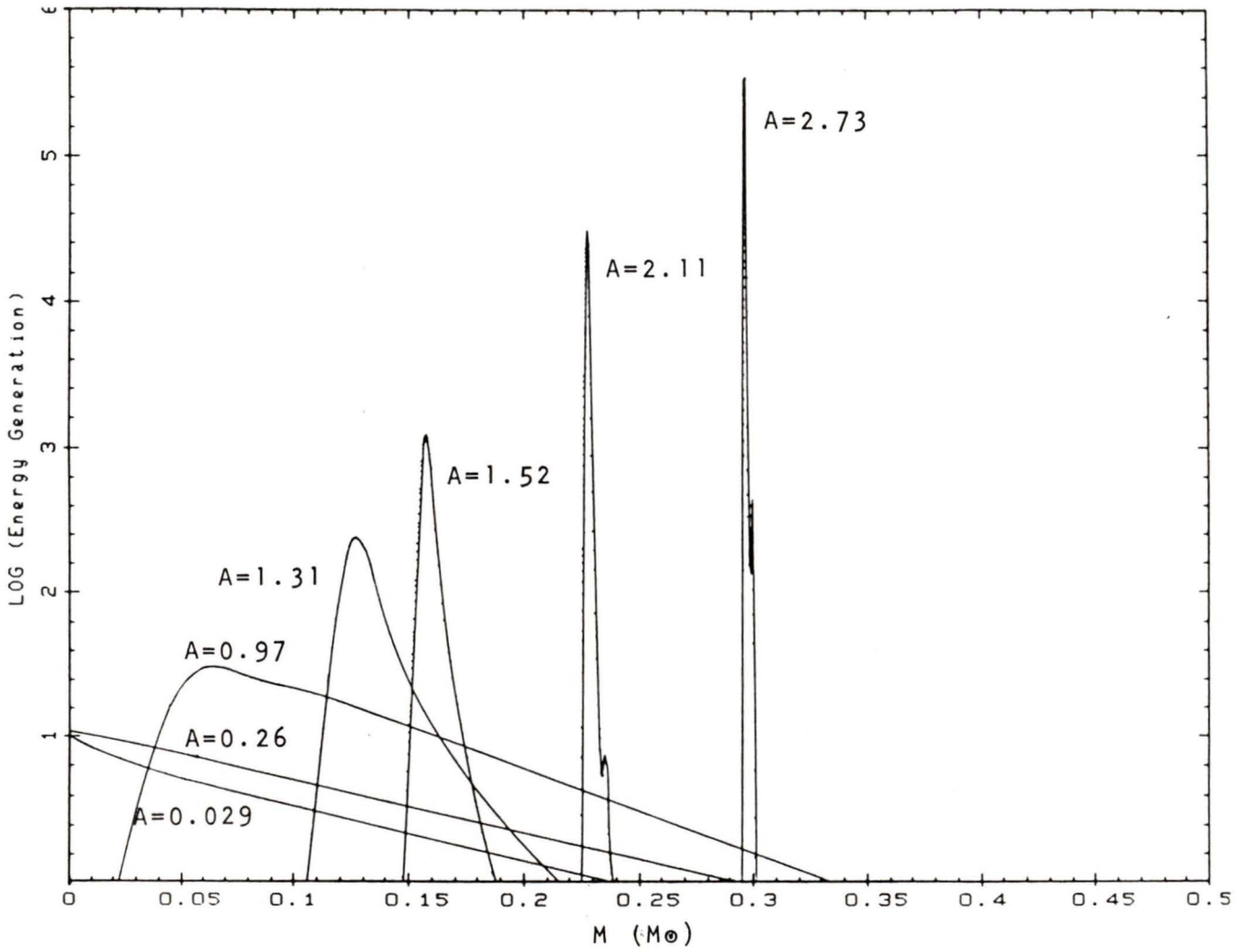

Figure 11: Energy generation profile for R4 at seven different ages. Only the innermost 0.5 M⊙ of the model star is plotted.

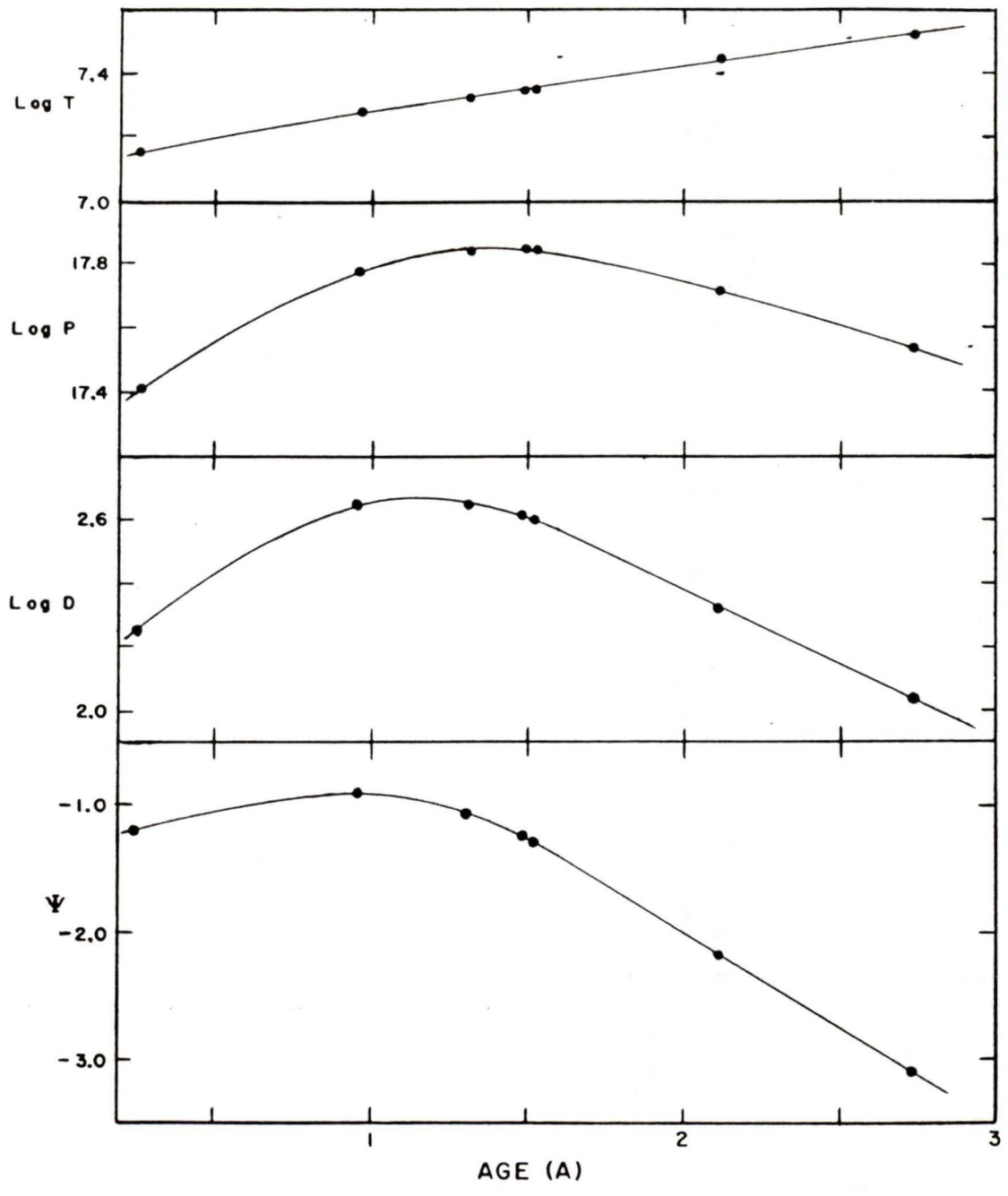

Figure 12: T, P, D, and Ψ versus age for R4.

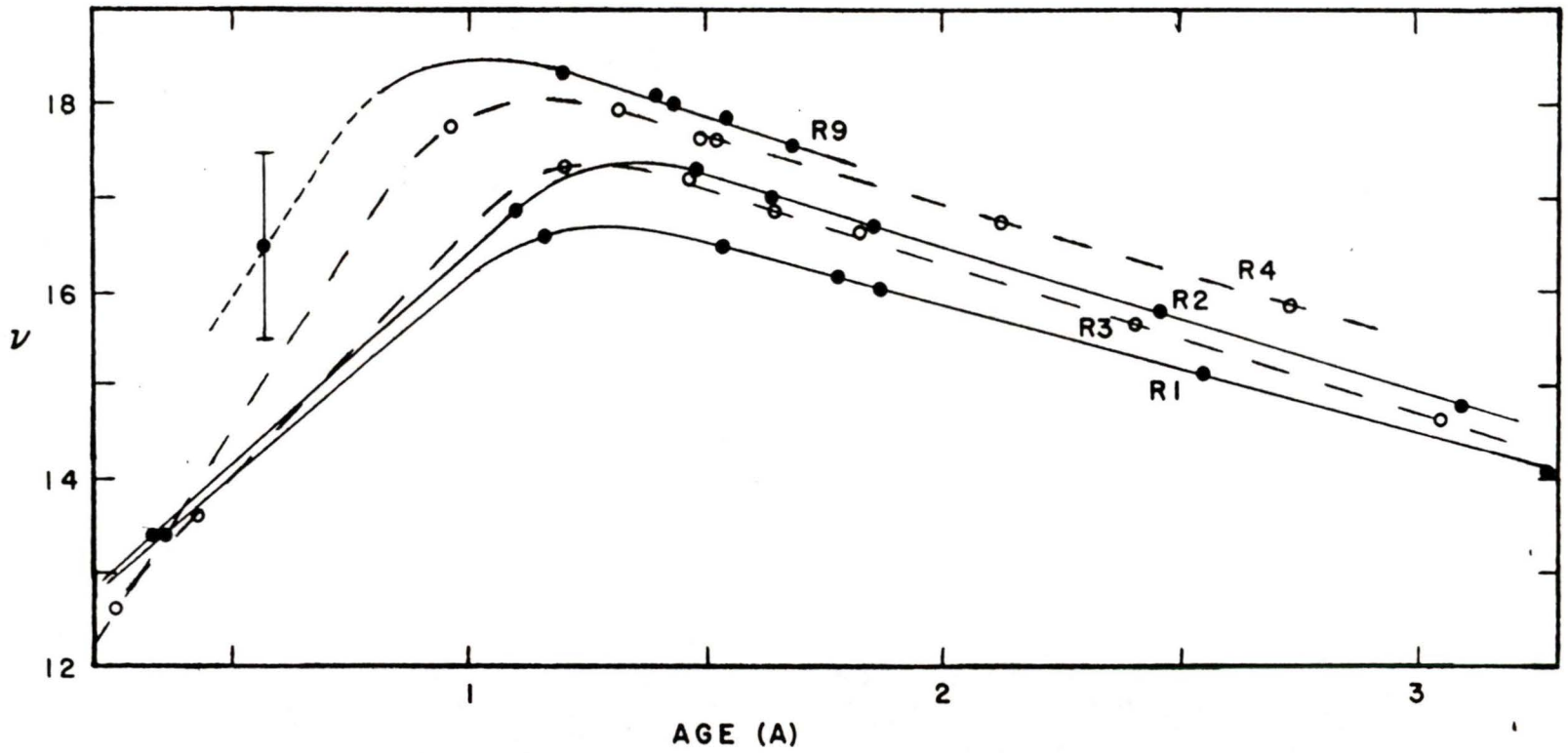

Figure 13: Temperature dependence of the nuclear burning rate, υ, in the shell versus age.

between ϵ and T: U actually has a mild inverse dependence on T, such that a higher T yields a lower U (see for example Schwarzschild 1958, p. 83). Therefore the models with the coolest shells have the highest U. This does not explain the rapid rise to a peak, however.

Several elements also exhibit maxima or minima in the region of A = 1.1 - 1.6, such as ^{12}C, ^{13}C, ^{4}He, and hydrogen. These may be simply due to the peaking of U, as they are all involved in the CNO cycle.

b) Eigensolutions

The eigensolution, as defined in Chapter 3, shows how the layers of the star react to a perturbation described by the eigenparameter, in the form of changes to the temperature, pressure, radius, and luminosity. Figure 14 shows the evolution of the solution for star R1. As one of the elements is always arbitrary, the surface pressure perturbation is set equal to 1. Two aspects are noteworthy.

First, the shell itself undergoes very little change at all times when subjected to a perturbation. The regions immediately above and below it become very active, however, by the time the shell is well developed. The material above the shell is infalling, heating up and increasing in

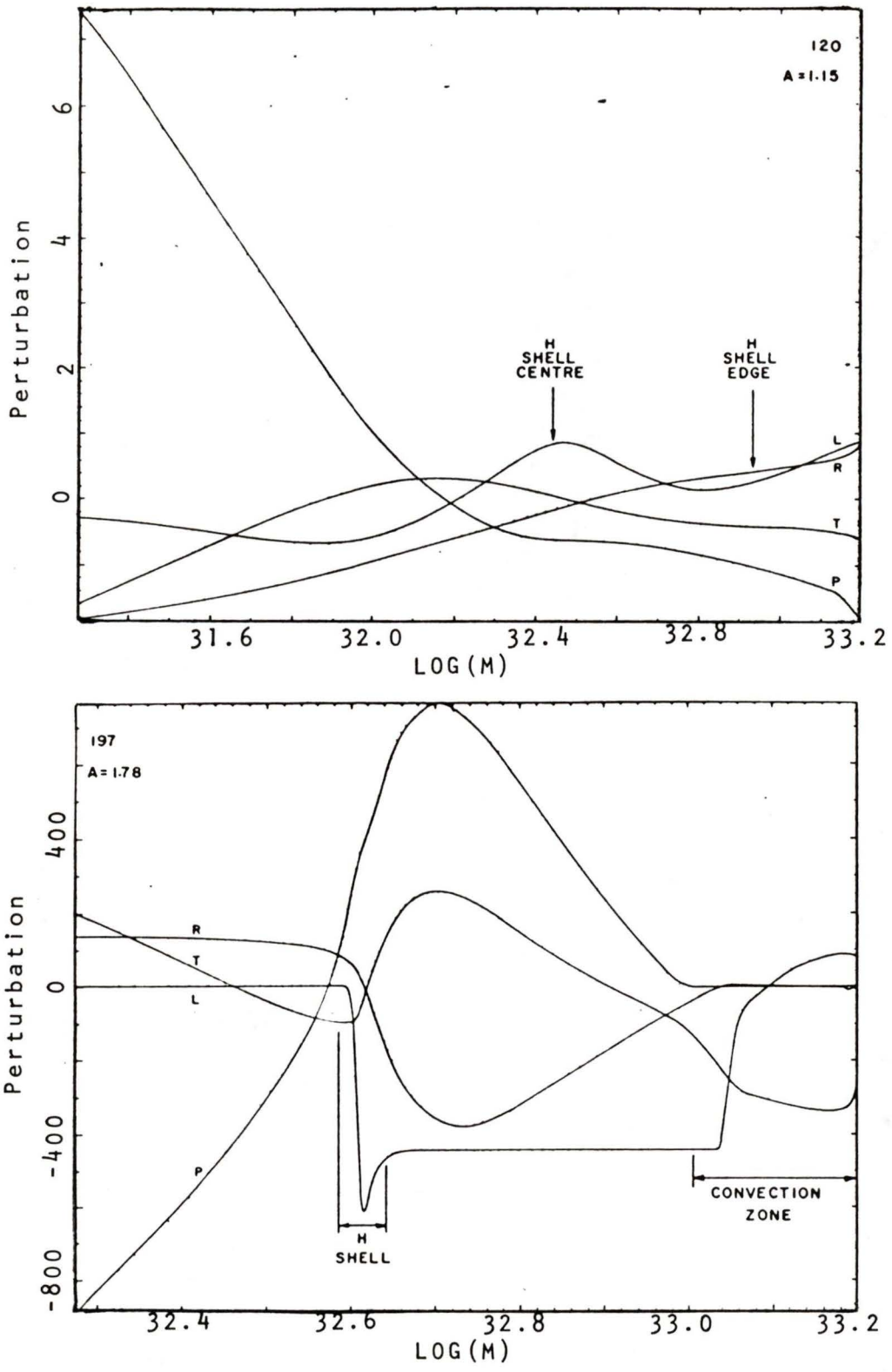

Figure 14: Eigensolutions for 4 models of star R1. P stands for δLog f (where f is a function of P used in the stellar model code), T for δLog T, R for δLog R, and L for δ(Lr/L). Mass is in grams, Log(M)=33.2 is the surface of R1. Continued.

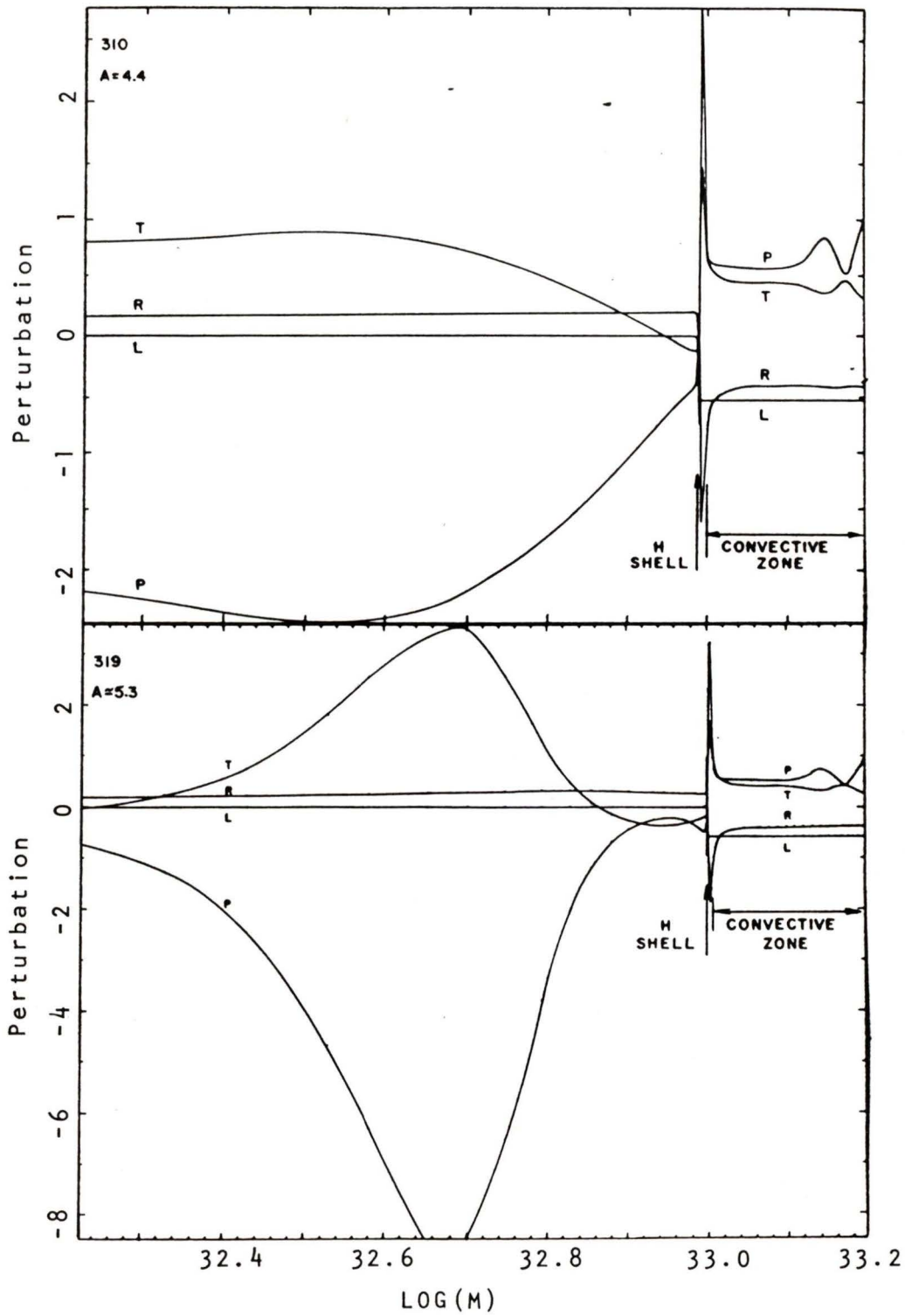

Figure 14: Continued.

pressure, while that below is rising, cooling, and decreasing in pressure.

Second, the lower part of the convective envelope is also relatively stable. By the time the model is on its way up the RGB (model 310), this zone is so close to the hydrogen shell that some interaction between the two may be occurring.

c) The convective envelope

The close proximity of the convective zone to the shell makes the former worth examining in some detail. Figure 15 shows the depth to which convection extends in the models. Compare this to Figure 7: they are quite close to being mirror images of each other, other than a difference in A of about .45 and R2 and R3 being reversed. These two stars differ so little in the two diagrams, however, that the slight reversal is within the uncertainty of the calculation. It is quite evident that the stars that become the least stable are those whose envelopes reach the deepest.

While a considerable correspondence seems to exist between the depth of the convective envelope and the stability of a star, it does not necessarily follow that one causes the other. Convection occurs when the radiative

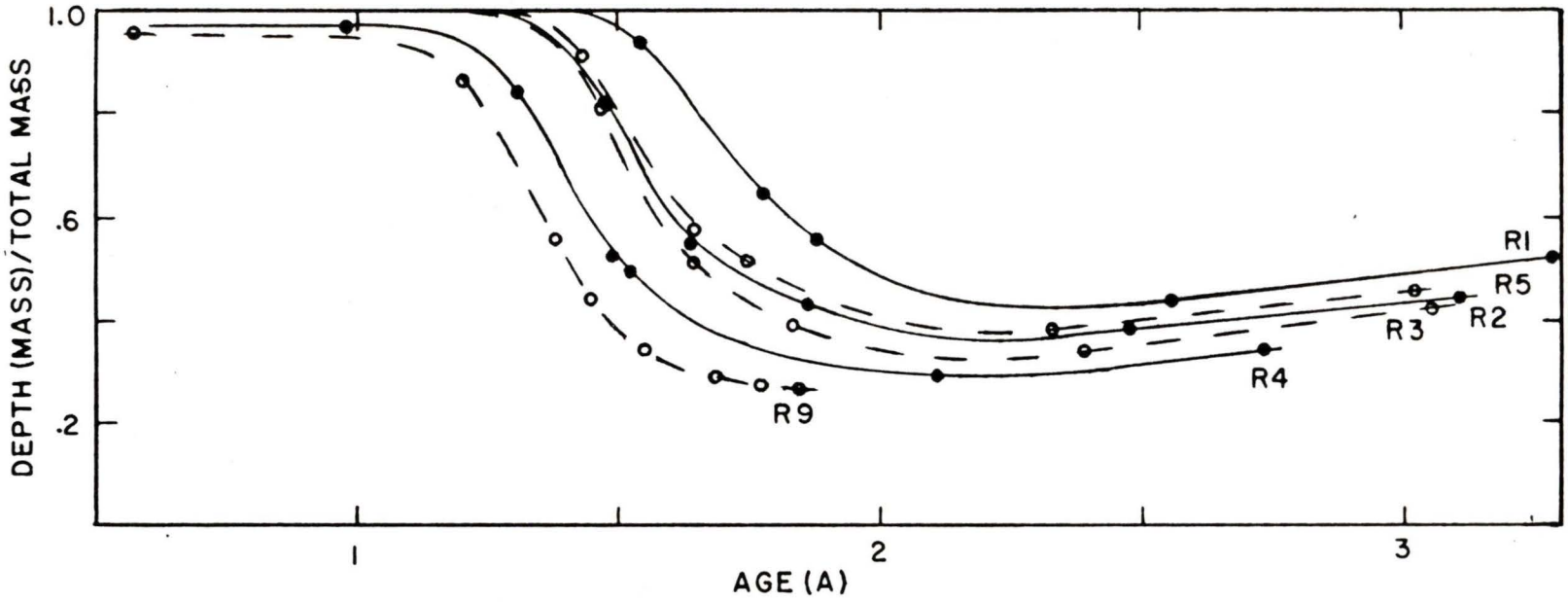

Figure 15: Convective envelope depth versus age. Depth is in terms of the mass enclosed by the envelope.

temperature gradient becomes excessive (see equation 7), so that the surface temperature or total radius of a star could be a factor in determining the depth to which convection goes. As Figure 6 shows, the least stable stars have the lowest effective temperatures, which is a direct result of the high metal content of the stars. So the sensitivity of the results in both Figures 7 and 15 to metallicity seems quite reasonable.

Another possible explanation for the similarity is revealed in Figure 16, which shows the envelope's position in the model as a function of the shell's position, both in terms of the mass that they enclose. It is almost as if the interaction is simply due to the shell getting in the way of the downward progression of the envelope, eventually pushing it back upwards as the star evolves up the RGB.

Nevertheless a test was made as to what effect the depth of the envelope has on τ. Two models were constructed with a minor modification in the mixing-length parameter, α. This value governs the efficiency of convection, and thus should be a means by which to increase or decrease the depth to which the convective layer reaches. The change in the depth of the zone and the largest zero are given in Table 3. While the depth of the zone does have some effect on τ, the small change in both quantities over such a range of τ (which is far greater than the range of roughly 1.5 to 1.7 which seems to be indicated as being

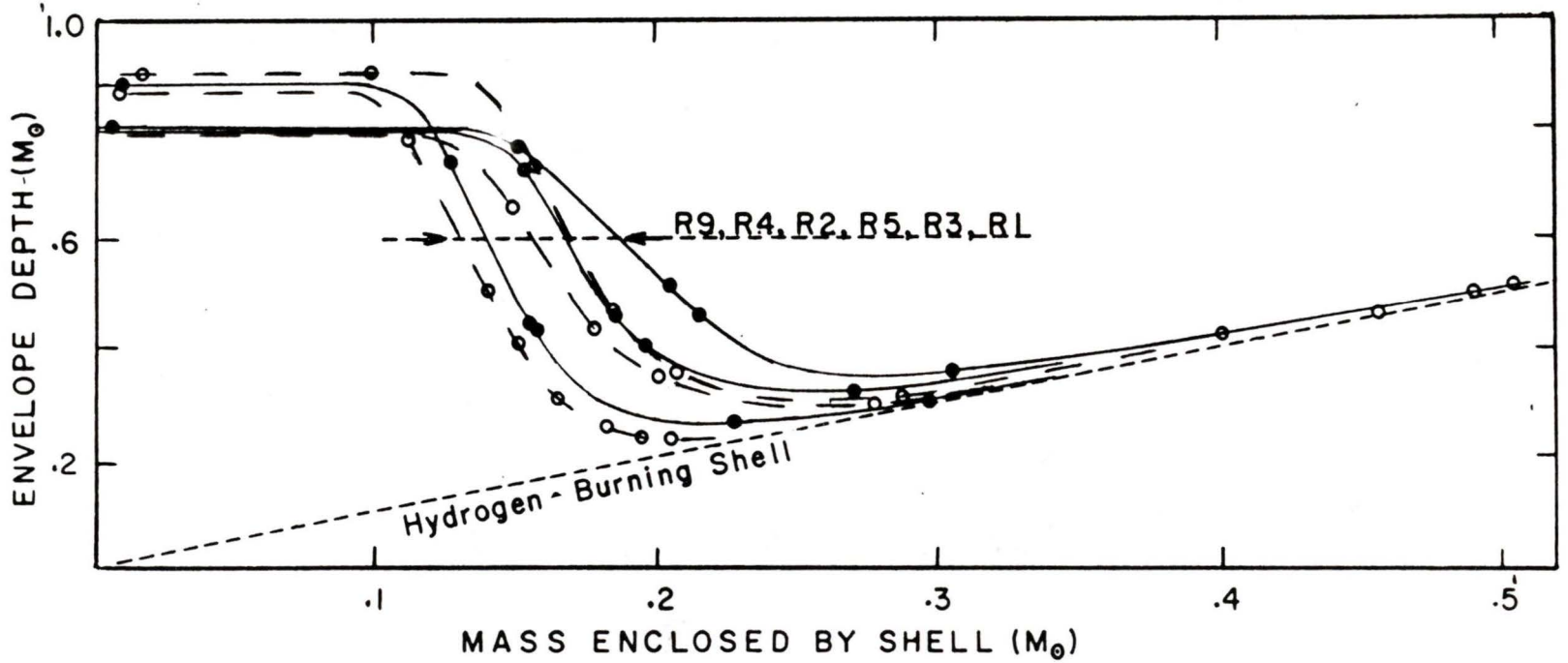

Figure 16: Convective envelope depth versus shell position. Depth is in terms of the mass enclosed by the envelope. Position of shell is also shown.

Table 3: Effects of changing α

Star	Mass ($M_\odot$)	Xo	Yo	Zo	α	At base of RGB: Log $(-\tau)$	At base of RGB: Depth of Envelope ($M_\odot$)
R3	0.9	0.799	0.2	0.001	1.6	7.72	0.51
R7	0.9	0.799	0.2	0.001	1.0	7.74	0.51
R8	0.9	0.799	0.2	0.001	2.5	7.71	0.53

realistic in stars by the intercomparison of observed and synthetic CMDs: see VandenBerg 1983) renders this a fairly poor test. The reason seems to be that α also influences the surface temperature appreciably. For example, decreasing α from 1.6 to 1.0 decreases the effective temperature by about 11% which increases the overall temperature gradient between the shell and the surface and therefore increases the depth of the convective zone. This apparently counteracts to a large degree the desired result of decreasing the depth via decreased efficiency.

5. Summary

Figure 17 summarizes all the significant events that occur near or at the base of the RGB. Most of these peak shortly before τ does, with the exception of the conditional equations and the convective envelope depth. Three groupings are apparent.

In the region of A = 1.0 - 1.5, the structure of the shell undergoes a major transition. This is the phase between the turn off point and the base of the RGB. Steadily increasing compression of the shell reverses, as revealed by the maxima of P, D, and ψ. This might be the cause of the peak in U which also occurs at the same time. The maxima and minima in the abundances of the various CNO cycle elements may be connected to the changes in U, as the abundances and U are connected through the energy generation rate. The convective envelope also starts to expand inwards after the turnoff point.

As these events do not coincide with the point of least stability, it does not seem as if they can be direct causes of such. However, BE identify U as the primary key to instability, and the maxima of both U and τ do vary with time in tandem from star to star. Higher U probably results in thinner shells, as ϵ (the profile of which defines the shell) would be more sensitive to the temperature change

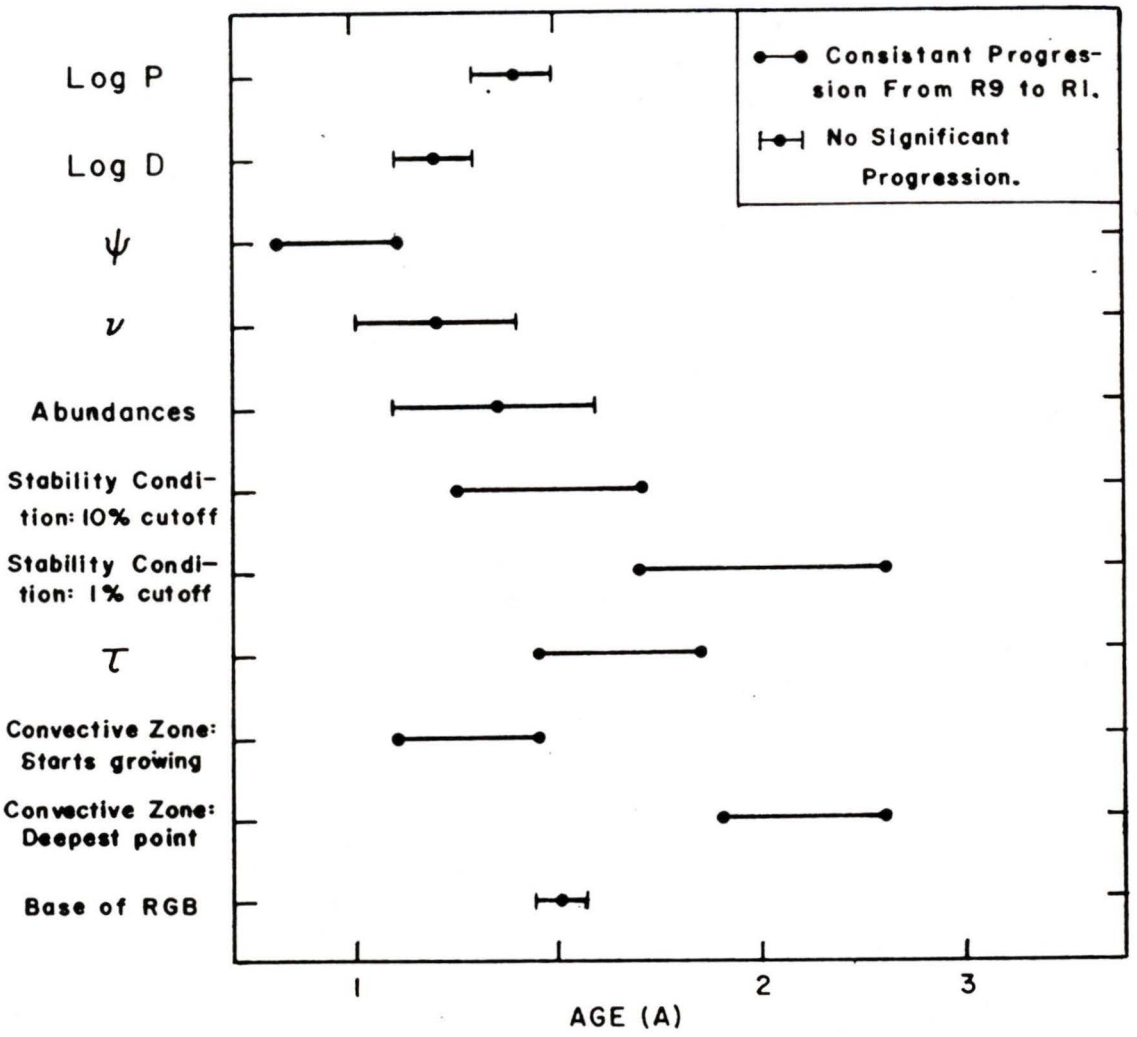

Figure 17: Summary of significant events near the base of the RGB. Parameters exhibit maxima or minima, or events occur at the indicated age. Six show a fairly consistant progression between stars: R9, R4, R3, R2, R5, R1 (or with R2 and R3 reversed). The other five do not show any significant progression.

across the shell and thus drop off more rapidly. As the stars with the thinnest shells are the least stable, the importance of U is confirmed. To achieve instability, it would seem that higher U or a delay in the peaking of U is required.

Well past the base of the RGB ($A \gtrsim 1.9$) the convective envelope reaches its deepest point in the star, and starts to closely precede the shell outwards. Despite the marvelously similar nature of Figures (7) and (15), it does not seem that the envelope causes instability or vice versa. Rather, the metallicity of the model probably determines the extent of both.

At the base of the RGB ($A = 1.3 - 1.8$), the point of least stability is predicted and found. While the derived conditions of stability described by equations (15) and (43) depend significantly on the definition of the boundary of the shell, they clearly show where the point of least stability occurs and its earlier occurence for the less stable stars. Thus the theory outlined in part 2 must be a good appproximation to reality. The location of this point is quite noteworthy as it is close to where the anomalous gaps in CMDs of clusters lie, such as the one shown in Figure 1. Whether or not a thermal instability could cause such a feature is not known at present, as no unstable models were created which could be studied in detail.

Thus the occurence of the tendency towards instability is due to the shell being thick enough to minimize radiative losses (by spanning a large change in temperature) yet thin enough to not affect the hydrostatic structure of the star if it is perturbed. The shell's thickness decreases considerably as the star evolves, passing through this crucial range, so a point of least stability is inevitable. But the degree of this tendency, and whether or not it ever reaches instability, seems to be strongly correlated with Z. Stability of the shell depends on how quickly it becomes thin, which is determined by U. U in turn depends on the shell's temperature, and directly or not this is probably determined by the metal content of the star. The star's mass and helium content have a much smaller effect on stability, but probably do so via the same intermediary parameters as Z does. Complex instability, as found to occur in helium shells, does not seem to be a likely outcome in hydrogen shells.

The theoretical conditions for instability outlined by SH and in Chapter 2 are verified. However BE's determination of the significance of U is confirmed qualitatively only, as the models studied here do not become oscillatorily unstable as they have predicted.

Two noteable factors that could influence stability, rotation and mass-loss, remain unexamined. Rotation has been identified as a potentially destabilizing factor

(Hartwick 1976), and its occurence might be able to "push" a star like R9 or R4 into instability. Mass loss on the RGB might also have this effect, by reducing the weight exerted by the envelope on the shell. Both of these require significant additions to the stellar evolution code to model them accurately, and therefore have not been investigated here.

It would also be of use to create one model star that does become unstable, however unrealistic a lifespan it might have. It would then be possible to observe the transition from stability to instability and determine how close more realistic models come to being unstable. Furthermore, such a model could be used to determine the observational consequences of instability, to see whether or not it could account for the gaps observed in some CMDs.

Bibliography

Armandroff, T.E. and Demarque, P. 1984, Astr. Ap., 139, 305.

Bolton, A. J. C. and Eggleton, P. P. 1973, Astr. Ap., 24, 429 (BE).

Boyce, W.E. and DiPrima, R.C. 1977, in Elementary Differential Equations and Boundary Value Problems (New York: John Wiley & Sons), p. 331-333.

Buonanno, R., Corsi, C.E., Fusi Pecci, R., Alcaino, G., and Liller, W. 1984, Astr. Ap. Suppl. 57, 75.

Cannon, R.D. 1984, in Observational Tests of the Stellar Evolution Theory, IAU Symp. 105, 123.

Cohen, J.G. and Phillips, A.C. 1980, Ap. J., 237, 99.

Cox, J.P. and Giuli, R.T. 1968, in Principles of Stellar Structure (New York: Gordon & Breach), p.420.

Dennis, T. R. 1971, Ap. J., 167, 311.

Freeman, K. C. and Norris, J. 1981, Ann. Rev. Astr. Ap., 19, 319.

Härm, R. and Schwarzschild, M. 1972, Ap. J., 172, 403 (HS).

Hartwick, F.D.A. 1976, B. A. A. S., 8, 265.

Henyey, L. G., Forbes, J. E., and Gould, N. L. 1964, Ap. J., 139,306.

Kippenhahn, R. and Thomas, H.-C. 1983, Astr. Ap., 124, 206.

Kippenhahn, R., Weigert, A., and Hofmeister, E. 1967, in Methods in Computational Physics, Vol.7, ed. B. Adler, S. Fernbach, and M. Rotenberg (New York: Academic), p. 129.

Law, W.-Y. 1981, Astr. Ap., 102, 178.

Novotny, E. 1973, in Introduction to Stellar Atmospheres and

Interiors (London: Oxford University Press), p.171-172.

Schwarzschild, M. 1958, in Structure and Evolution of the Stars (New York: Dover Publications).

Schwarzschild, M. and Härm, R. 1965, Ap. J., 142, 855 (SH).

VandenBerg, D. A. 1983, Ap. J. Suppl., 51, 29.

Appendix I: Computer Code for Finding Eigenparameters

Data files required

The routine listed below requires as its primary input the matrix of coefficients describing the model star from the four differential equations (3) to (6) for each of the n-1 layers between the n grid points, as well as for the four boundary conditions. It also requires an array containing the special set of coefficients that allow the introduction of the eigenparameter, which occurs in equation (4) for each layer. This extra set could be directly incorporated into the array of coefficients in the main stellar model code if desired, but keeping the two separate reduces the changes that must be made to the code.

One can write the gravitational term of the thermal equation (5) more precisely as

$$\epsilon_g = -T\frac{dS}{dT} - \sum_i \eta_i \frac{d}{idt}\left(\frac{n_i}{D}\right) \qquad (66)$$

where η_i is the chemical potential and n_i is the number per unit mass of the ith kind of particle, and dt is the time step between consecutive models (see Cox and Giuli, 1968). Then, if equation (45) is written as

$$f = \frac{dL}{dM} = (\epsilon_t + \epsilon_g + \epsilon_n) \tag{67}$$

(where ϵ_t is the nuclear-burning energy generation rate and ϵ_n is the energy loss due to nutrinos) and the corresponding difference equation as

$$F = \frac{L_{i+1} - L_i}{M_{i+1} - M_i} - \frac{f_{i+1} + f_i}{2}, \tag{68}$$

the "corrections" equation is

$$0 = F + \frac{dF}{dR_i}\delta R_i + \frac{dF}{dR_{i+1}}\delta R_{i+1} + \cdots \frac{dF}{dT_{i+1}}\delta T_{i+1}, \tag{69}$$

where the δ's represent the desired unknowns. Similarily, the coefficients associated with the eigenparameter can be obtained by writing

$$\epsilon_{eig} = -T\frac{dS}{dT} \tag{70}$$

$$f' = \epsilon_{eig} \tag{71}$$

$$F' = -\frac{f'_{i+1} + f'_i}{2} \tag{72}$$

$$0 = F' + \frac{dF'}{dR_i}\delta R_i + \frac{dF'}{dR_{i+1}}\delta R_{i+1} + \cdots \frac{dF'}{dT_{i+1}}\delta T_{i+1}. \qquad (73)$$

These coefficients are incorporated into the array with the main coefficients generated by the normal stellar code by considering equation (61):

$$\delta\left(\frac{dL}{dM}\right) = \delta\epsilon - \delta(T)\cdot\frac{dS}{dt} + T\frac{\delta(S)}{\tau} \qquad (61)$$

If there were no perturbation, the last term would be $T\frac{\delta(S)}{\Delta t}$: this is what the normal stellar code uses. Therefore, to the main coefficients one must add those generated by equation (61) times $(\Delta t/\tau - 1)$. This procedure is done in subroutine DET.

The format of the data used by the routine is as follows, where NMESH is the number of grid points:

```
(((AR(I,J,K), K=1,4), AR2(I,J), J=1,9), I=2,NMESH),
((SAV1(I,J), SAV2(I,J), J=1,2), SAV3(I), I=1,5)
```

where:

AR(I,J,K) contains the I = 2, NMESH 4x9 arrays in the form

$$\frac{dF_R}{dR_i}, \frac{dF_R}{dL_i}, \frac{dF_R}{dP_i}, \frac{dF_R}{dT_i}, \frac{dF_R}{dR_{i+1}}, \frac{dF_R}{dL_{i+1}}, \frac{dF_R}{dP_{i+1}}, \frac{dF_R}{dT_{i+1}}, -F_R$$

$$\frac{dF_L}{dR_i}, \frac{dF_L}{dL_i}, \frac{dF_L}{dP_i}, \frac{dF_L}{dT_i}, \frac{dF_L}{dR_{i+1}}, \frac{dF_L}{dL_{i+1}}, \frac{dF_L}{dP_{i+1}}, \frac{dF_L}{dT_{i+1}}, -F_L$$

$$\frac{dF_P}{dR_i}, \frac{dF_P}{dL_i}, \frac{dF_P}{dP_i}, \frac{dF_P}{dT_i}, \frac{dF_P}{dR_{i+1}}, \frac{dF_P}{dL_{i+1}}, \frac{dF_P}{dP_{i+1}}, \frac{dF_P}{dT_{i+1}}, -F_P$$

$$\frac{dF_T}{dR_i}, \frac{dF_T}{dL_i}, \frac{dF_T}{dP_i}, \frac{dF_T}{dT_i}, \frac{dF_T}{dR_{i+1}}, \frac{dF_T}{dL_{i+1}}, \frac{dF_T}{dP_{i+1}}, \frac{dF_T}{dT_{i+1}}, -F_T$$

AR2(I,J) contains the I = 2, NMESH 1x9 arrays with the eigenvalue coefficients in the form

$$\frac{dF'}{dR_i}, \frac{dF'}{dL_i}, \frac{dF'}{dP_i}, \frac{dF'}{dT_i}, \frac{dF'}{dR_{i+1}}, \frac{dF'}{dL_{i+1}}, \frac{dF'}{dP_{i+1}}, \frac{dF'}{dT_{i+1}}, -F'$$

SAV1(I,J) contains the 2x5 surface boundary condition coefficients, in the form

$$\frac{dF_1}{dR_i}, \frac{dF_1}{dL_i}, \frac{dF_1}{dP_i}, \frac{dF_1}{dT_i}, -F_1$$

$$\frac{dF_2}{dR_i}, \frac{dF_2}{dL_i}, \frac{dF_2}{dP_i}, \frac{dF_2}{dT_i}, -F_2$$

SAV2(I,J) contains the 2x5 central boundary condition coefficients, in the form

$$\frac{dF_1}{dR_i}, \frac{dF_1}{dL_i}, \frac{dF_1}{dP_i}, \frac{dF_1}{dT_i}, -F_1$$

$$\frac{dF_2}{dR_i}, \frac{dF_2}{dL_i}, \frac{dF_2}{dP_i}, \frac{dF_2}{dT_i}, -F_2$$

and SAV3(I) contains the 1x5 central boundary condition eigenvalue coefficients, in the form

$$\frac{dF'}{dR_i}, \frac{dF'}{dL_i}, \frac{dF'}{dP_i}, \frac{dF'}{dT_i}, -F' \ .$$

The second data file required outlines where on the complex plane of the eigenparameter the search for zeros should be conducted. A grid pattern is used, along which the determinant is calculated so as to find sign changes of its real and imaginary components. The grid pattern is shown in Figure 18. The data file is in the following form:

```
R1,  R2,  R3,  R4
I1,  I2,  I3,  I4
S1,  S2
IDEBug
'IHEADing', DELT
```

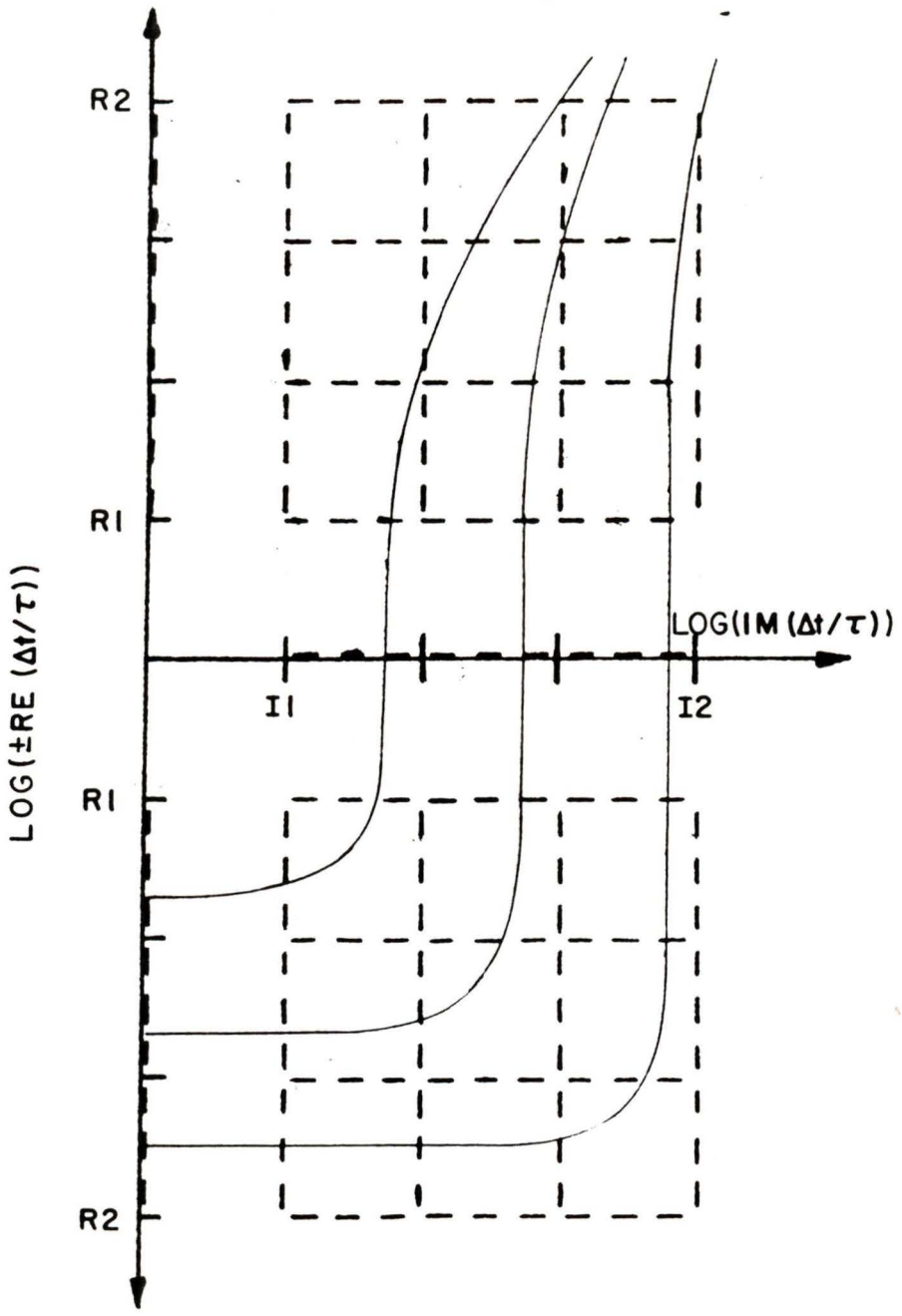

Figure 18: Grid search pattern used by CONTROL to locate sign changes of real and imaginary components of determinant on the complex $\Delta t/\tau$ plane.

where:

R1, R2, I1, and I2 are as indicated in Figure 18.

R3 and I3 are the logarithms of the inverse of the grid line spacings for lines running parallel to the Imaginary and Real axes respectively (i.e. how many lines over an interval of 1 in the logarithm).

R4 and I4 are the logarithms of the inverse of the grid point spacings along grid lines running parallel to the Real and Imaginary axes respectively (i.e. how many points over an interval of 1 in the logarithm). 80 is felt to be optimum for both, resulting in a grid point spacing that is fine enough to catch all significant features and yet not be overly detailed (however, not much experimentation has been done as to what the smallest value is that one can use in different situations).

S1 and S2 are the first and last grid line patterns to be run, the patterns being as follows:

1. lines running +R1 -> +R2, imag. components > 0
2. lines running +I1 -> +I2, real components > 0
3. lines running -R1 -> -R2, imag. components > 0
4. lines running +I1 -> +I2, real components < 0
5. lines running +R1 -> +R2, imag. component = 0

6. lines running +I1 -> +I2, real component = 0

7. lines running -R1 -> -R2, imag. component = 0

(Note that the half of the complex plane having the imaginary component negative is just the mirror image of the the positive half, and is therefore ignored).

IDEBug is a debugging and control flag, having the following effects:

Value	Find routine used	Debugging output?
0	FIND	No
1	FINDIQ	No
2	FINDALL	No
3	FIND	Yes
4	FINDIQ	Yes
5	FINDALL	Yes

IHEADing is a label that is printed at the bottom the the output file (maximum 20 characters, and must be placed inside quotes).

DELT is the time step in years used between the present and previous models. It is used in the calculation of the time derivative of the entropy S, and is part of the definition of the eigenvalue $\Delta t/\tau$. It should be significantly less than the

timestep used to evolve the model to its present point.

As an example, consider the file:

```
0.1, 10.0,  4,  80
0.1, 100.0, 1,  80
3, 7
0
'Test', 1E7
```

This would result in a grid pattern as shown in Figure 19.

The Programs

The eigenparameter code is divided into one main program and six subroutines. They are as follows:

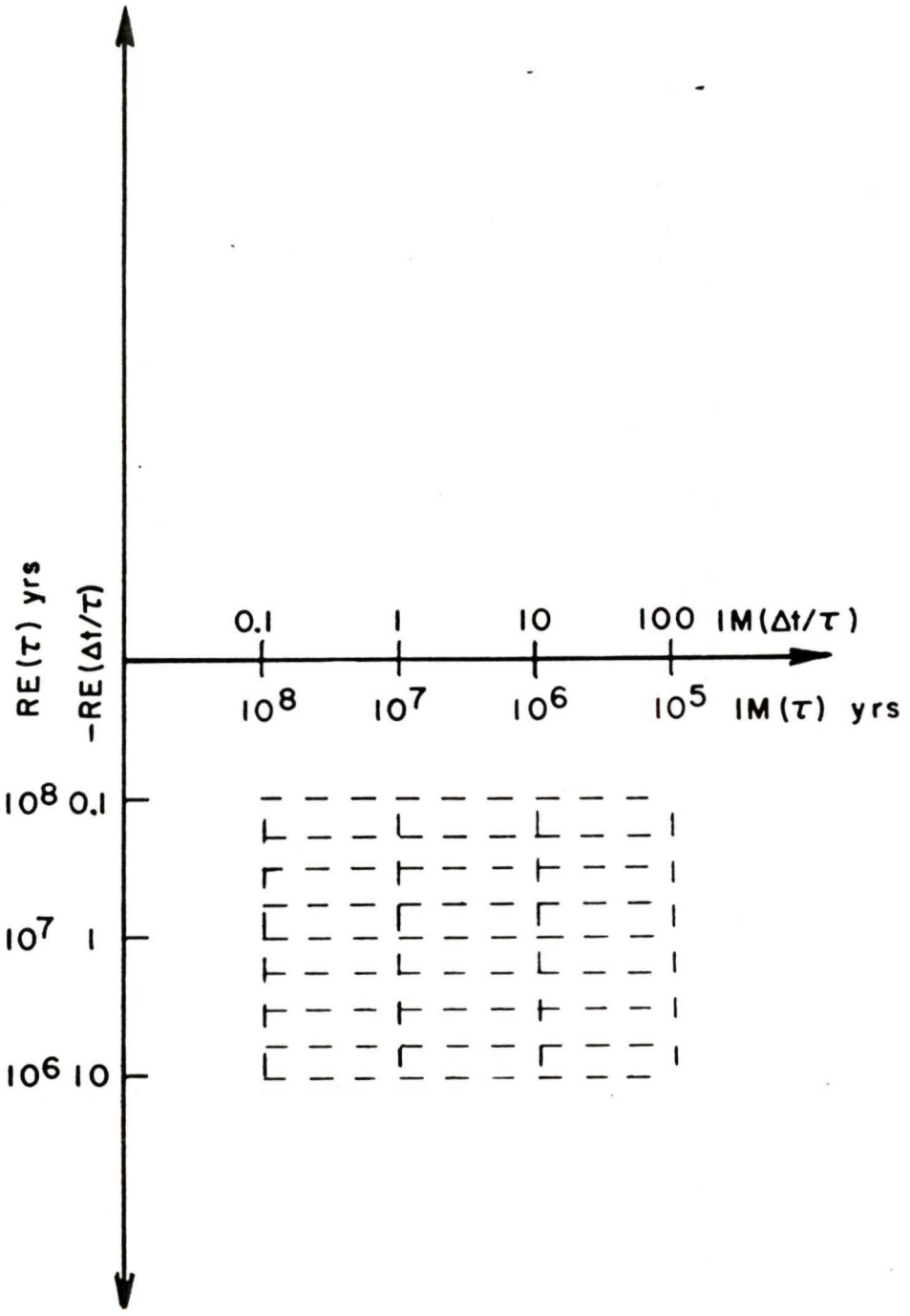

Figure 19: Sample grid search pattern. See text for data file represented.

```
C                    ******* MAIN PROGRAM *******
C
C  Input files are 30 (run parameters) and 31 (coefficient arrays)
C  Output file is 19
C
C  Uses STOREd arrays of coefficients describing models created by REDX1
C    and finds sign changes in the determinant for trial eigen-parameter
C    values, to locate zeros.  Input file 30 specifies over what region
C    of complex e-parameter plane to search.  Output is a listing along
C    grid lines of where the real and imaginary part of the determinat
C    changes sign, in this format:
C
C  R(eigenp.)  I(eigenp.)    cos(deter) sin(deter)    magn(deter)     F
C
C    where F=1 for a real part sign change, =2 for an imaginary part
C    sign change, =3 for both sign changes, and =0 for no sign change.
C
C  See also DETERM.DOC for instructions on setting up input file 30.
C
      INTEGER*2 C,C2,S1,S2,IDEB,FLRI(7),FLS(7),FLA(7)
      INTEGER NROWS(2)
      CHARACTER*20 IHEAD
      INTEGER TALLY
      REAL RWSTEP(2),R,I,RE(4),IM(4)
      DOUBLE PRECISION AR(400,9,4),AR2(400,9),SAV1(5,2),
     1  SAV2(5,2),SAV3(5)
      DATA N2/9/,N77/7/
      COMMON /ARRAY/ AR,AR2,SAV1,SAV2,SAV3
      COMMON /ARRAY2/ NMESH,NBC,NDE,N3,N4,N5,N6,N7,N2,N77
      COMMON /DEBUG/ IDEB
      COMMON /TAL/ TALLY
C
      WRITE(19,3)
      WRITE(19,4)
 3    FORMAT(11X,' Eigen Value',16X,'Determinant',3X,'LOG (Magn.)')
 4    FORMAT (2X,63('-'))
      READ (30,*) (RE(I),I=1,4),(IM(I),I=1,4),S1,S2,IDEB
      READ (30,*) IHEAD,DELT
      READ (31,*) NMESH,NBC,NDE,N3,N4,N5,N6,N7
      READ (31,*) (((AR(I,J,K),K=1,4),AR2(I,J),J=1,9),I=2,NMESH)
     1      ,((SAV1(I,J),SAV2(I,J),J=1,2),SAV3(I),I=1,5)
C
C
C     Setting up grid pattern of e-param (EIG=(Real,Imag)=dT/tau):
C     NROWS(i) = number of grid rows: i=1 for real track, 2 for imag.
C     RWSTEP(i) = step size along grid row. i=1 for imag, =2 for real.
      NROWS(1)= ALOG10(IM(2)/IM(1)) * IM(3)
      NROWS(2)= ALOG10(RE(2)/RE(1)) * RE(3)
      RWSTEP(1)= 10**(1/IM(3))
      RWSTEP(2)= 10**(1/RE(3))
```

```
      DO 100 C = 1, 7
        FLRI(C)=1
        IF (C.EQ.(2*(C/2))) FLRI(C)=2
        FLS(C)=1
        C2=(C-1)/2
        IF (C2.NE.(2*(C2/2))) FLS(C)=-1
        FLA(C)=1
        IF (C.GE.5) FLA(C)=0
 100    CONTINUE
C
C   Main loop:  Counter C determines what part of plane to search in,
C     as specified by inputted range of S1 to S2.  R is real part of
C     e-parameter, I is imag part.  LAST is the last value of either
C     R or I along a grid line.  STP is grid point step size.  FLRI(c)
C     indicates whether grid line is parallel to the R or I axis.  IMX
C     is the maximum number of grid points that can be jumped ahead
C     at a time.
C   FINDIQ, FIND, and FINDALL are three different methods of searching.
C     FINDIQ attempts to interpolate sign crossing positions, and is
C     not yet perfected.  FIND is less "intelligent", but is the
C     best way.  FINDALL prints out every grid point, used to show
C     the progression of determinant along a grid line.
C
      DO 200 C = S1, S2
       NR=NROWS(FLRI(C))*FLA(C)
       DO 130 IR = 0, NR
        IF (FLRI(C).EQ.1) THEN
          R= FLS(C) * RE(1)
          I= FLA(C) * IM(1)*RWSTEP(1)**IR
          STP= 10**(1/RE(4))
          LAST= ALOG10(RE(2)/RE(1))*RE(4)
        ELSE
          R= FLS(C)*FLA(C) * RE(1)*RWSTEP(2)**IR
          I= IM(1)
          STP= 10**(1/IM(4))
          LAST= ALOG10(IM(2)/IM(1))*IM(4)
        END IF
        IMX=8.
        IF (IDEB-1-3*(IDEB/3)) 105, 110, 115
 105    CALL FIND(R,I,LAST,STP,FLRI(C),IMX)
        GOTO 130
 110    IF ((C.EQ.5).OR.(C.EQ.7)) GOTO 105
        CALL FINDIQ(R,I,LAST,STP,FLRI(C),IMX)
        GOTO 130
 115    CALL FINDALL(R,I,LAST,STP,FLRI(C))
 130    CONTINUE
 200   CONTINUE
      WRITE (19,240)
 240  FORMAT(6(' 0.,'))
      WRITE (19,250) IHEAD,DELT,TALLY
```

```
 250  FORMAT(A20,4X,'dT = ',E8.1,4X,'# of points used = ',I5)
      STOP
      END
C
C                      *******     OUTP     *******
C
      SUBROUTINE OUTP(DETA,DETM,EIG,IDEB,IFLAG)
      DOUBLE PRECISION DETA,DETM
      COMPLEX EIG
      INTEGER*2 IDEB,IFLAG
C
 115    IF (IFLAG.EQ.9) THEN
          DDETRE=-9.
          DDETIM=-9.
          GOTO 118
          END IF
        DDETIM=DSIN(DETA)
        IFLAG=0
        IF (ABS(DDETRE).LT.1.D-14) DDETRE=0.
        IF (ABS(DDETIM).LT.1.D-14) DDETIM=0.
        IF (IDEB-3*(IDEB/3).EQ.2) GOTO 117
        IF ((DDETRE*D1.GT.0.OR.DDETRE.EQ.D1).AND.
     1       (DDETIM*D2.GT.0.OR.DDETIM.EQ.D2)) GOTO 125
 117    IF (DDETRE*D1.LT.0.) IFLAG=1
        IF (DDETIM*D2.LT.0.) IFLAG=IFLAG+2
 118    WRITE (19,120) EIG,DDETRE,DDETIM,DETM,iflag
 120    FORMAT (2F15.6,4X,F8.5,', ',F8.5,2X,F7.2,2X,I1)
 125    D1=DDETRE
        D2=DDETIM
      RETURN
      END
C
C                      *******     FINDALL    *******
C
C  FINDALL obtains and prints the determinant at every point along the
C    grid line.
C
C  The determinant is stored in polar form:  deter = DETM*e**(i*DETA).
C    Thus the sign change in the real part occurs when DETA crosses
C    pi/2 or 3/2*pi, and in the imaginary part when it crosses pi or 0.
C
      SUBROUTINE FINDALL(R,I,LAST,STP,FLRI)
      REAL R,I
      INTEGER TALLY
      INTEGER*2 FLRI,IC,IFLAG,IDEB
      DOUBLE PRECISION DETA,DETM
      DOUBLE PRECISION AR(400,9,4),AR2(400,9),SAV1(5,2),
     1  SAV2(5,2),SAV3(5)
      COMPLEX EIG,DETER*16
      COMMON /ARRAY/ AR,AR2,SAV1,SAV2,SAV3
```

```
      COMMON /ARRAY2/ NMESH,NBC,NDE,N3,N4,N5,N6,N7,N2,N77
      COMMON /DETE/ DETER,DETA,DETM,IFLAG
      COMMON /DEBUG/ IDEB
      COMMON /TAL/ TALLY
      DO 140 IC = 0, LAST
        IF (FLRI.EQ.1) THEN
          EIG= CMPLX(R*STP**IC,I)
        ELSE
          EIG= CMPLX(R,I*STP**IC)
        END IF
        DETA=0.
        DETM=0.
        IFLAG=0
        CALL DET(EIG)
        CALL OUTP(DETA,DETM,EIG,IDEB,IFLAG)
 140    CONTINUE
      RETURN
      END
C
C                     *******     FIND     *******
C
C  FIND uses a binary search pattern to locate sign changes of the
C    components of the determinant, using a coarse step size of IMX0
C    grid points (typically 8).
C
C  The determinant is stored in polar form:  deter = DETM*e**(i*DETA).
C    Thus the sign change in the real part occurs when DETA crosses
C    pi/2 or 3/2*pi, and in the imaginary part when it crosses pi or 0.
C
      SUBROUTINE FIND(R,I,LAST,STP,FLRI,IMX0)
      REAL R,I
      INTEGER DELTC
      INTEGER TALLY
      INTEGER*2 FLRI,IC0,IC1,IC2,IFLAG,IDEB
      DOUBLE PRECISION DETA,DETM,DE1,DM1,DE2,DM2,PI
      DOUBLE PRECISION AR(400,9,4),AR2(400,9),SAV1(5,2),
     1  SAV2(5,2),SAV3(5)
      COMPLEX EIG,DETER*16
      COMMON /ARRAY/ AR,AR2,SAV1,SAV2,SAV3
      COMMON /ARRAY2/ NMESH,NBC,NDE,N3,N4,N5,N6,N7,N2,N77
      COMMON /DETE/ DETER,DETA,DETM,IFLAG
      COMMON /DEBUG/ IDEB
      COMMON /TAL/ TALLY
      PI= 3.1415926536
      PI2=PI/2.
      IC2=0
      IC0=0
      EIG=CMPLX(R,I)
      DETA=0.
      DETM=0.
```

```
      IFLAG=0
      CALL DET(EIG)
      CALL OUTP(DETA,DETM,EIG,IDEB,IFLAG)
      IF (IFLAG.EQ.9) GOTO 120
      DE1=DETA
      IQ1=DE1/PI2
      DM1=DETM
      IMX=IMXO
      DELTC=IMX/2
C
C  This is the starting point for eqch new grid point chosen.
C    DELTC = the number of grid points to jump ahead.
C    IC1, IC2 = the previous and present grid points.
C
 30   IC1=IC2
      IC2=IC2+DELTC
      IF (IC2.GT.LAST) THEN
        IF (IC1.GE.LAST) GOTO 150
        IC2=LAST
        DELTC=IC2-IC1
        END IF
 35   IF (FLRI.EQ.1) THEN
        EIG=CMPLX(R*STP**IC2,I)
       ELSE
        EIG=CMPLX(R,I*STP**IC2)
        END IF
      DETA=0.
      DETM=0.
      IFLAG=0
      CALL DET(EIG)
      IF (IFLAG.EQ.9) GOTO 120
      DE2=DETA
      IQ2=DE2/PI2
      DM2=DETM
 105  FORMAT(1X,2(F5.2,2X,I1,2X),2(2X,F6.2),4X,I2)
      IF (IQ1.NE.IQ2) GOTO 100
 60   DELTC=IMX
 70   DE1=DE2
      DM1=DM2
      IQ1=IQ2
      GOTO 30
C
C  Once a sign change has been detected between two grid points
C    (i.e. DETA has changed quadrant), one is sent to line 100.
C    Here, the gap between the previous and present grid points is
C    halved, and the above procedure continues until the gap is but
C    one grid point.
C
 100  IF (IABS(DELTC).EQ.1) GOTO 110
      IMX=(IMX+1)/2
```

```
        IC2=(IC2+IC1)/2
        DELTC=IC2-IC1
        GOTO 35
C
C  When the location of a sign change has been narrowed down to
C    lying between two adjacent grid points, one is sent to line 110.
C    IFLAG is set = 1 for a real-component sign change, = 2 for an
C    imaginary-component sign change, and = 3 if both components
C    change in sign.
C
       IF (DSIN(DE2)*DSIN(DE1).LT.0.) IFLAG=IFLAG+2
 120   CALL OUTP(DE2,DM2,EIG,IDEB,IFLAG)
       IMX=IMX0
       DELTC=MIN0(IMX/2,(IC2-IC0))
       IC0=IC2
       GOTO 70
 150   RETURN
       END
C
C                      *******     DET     *******
C
C  DET calculates the determinant given the large coefficient array
C    and a value for EIG (<>t/tau).  It breaks the large array back
C    into its 4x9 subarrays (or 2x5 arrays for the boundary conditions),
C    calculates the determinant for each one, and multiplies these
C    together to get the determinant for the entire array.
C
       SUBROUTINE DET(EIG)
       DOUBLE PRECISION DETERIM,DETERRE,DETA,DETM,AA1(2)
       DOUBLE PRECISION AR(400,9,4),AR2(400,9),SAV1(5,2),SAV2(5,2),
      1    SAV3(5)
       COMPLEX*16 EIG*8,DETER,SAV4(5,2),BC(9,4),AA(7,4),
      1    AR3(9,4),A(9),Y(5,2),z(5,4)
       INTEGER*2 IFLAG,IDEB
       INTEGER TALLY
       DATA N2/9/,N77/7/
       EQUIVALENCE (DETER,AA1,DETERRE),(AA1(2),DETERIM)
       COMMON /DETE/ DETER,DETA,DETM,IFLAG
       COMMON /DEBUG/ IDEB
       COMMON /ARRAY/ AR,AR2,SAV1,SAV2,SAV3
       COMMON /ARRAY2/ NMESH,NBC,NDE,N3,N4,N5,N6,N7,N2,N77
       COMMON /TAL/ TALLY
       TALLY=TALLY+1
C
C  SAV1 is the 2x5 array for the surface boundary conditions.
C
 10    DO 21 J=1,NBC
        DO 21 K=1,N3
 21       Y(K,J)=SAV1(K,J)
       CALL SIMEQDD(Y,15,N3,NBC)
```

```
        CALL DETADD
        DO 22 M=N4,N3
         DO 22 K=1,NBC
          BC(M,K)=-Y(M,K)
22        Y(M,K)=BC(M,K)
C
C  AR3 is a temporary array containing the coefficients in AR modified
C    by the introduction of the e-parameter coefficients in AR2 for the
C    current grid point II.
C
        DO 100 II=2,NMESH
         DO 25 J=1,9
          AR3(J,1)=AR(II,J,1)
          AR3(J,3)=AR(II,J,3)
          AR3(J,4)=AR(II,J,4)
          AR3(J,2)=AR(II,J,2)+(EIG-1.)*AR2(II,J)
25        CONTINUE
C
C  AA is a 4x7 array containing the partially row-reduced array AR3.
C
         DO 50 J=1,NDE
          DO 30 M=1,NDE
           L=M+NDE
           A(M)=AR3(M,J)
30         AA(M+N6,J)=AR3(L,J)
          A(N3)=AR3(N2,J)
          DO 40 M=1,N6
           K=M+NBC
           DO 35 L=1,NBC
35          A(K)=A(K)+Y(K,L)*A(L)
40         AA(M,J)=A(K)
          DO 45 L=1,NBC
45         A(N3)=A(N3)+Y(N3,L)*A(L)
50        AA(N77,J)=A(N3)
         CALL SIMEQDD(AA,15,N77,NDE)
         CALL DETADD
         IF (IFLAG.EQ.9) GOTO 115
         DO 60 L=1,N7
          K=L+NDE
          DO 55 J=1,NDE
55         BC(J,L)=-AA(K,J)
          K=L+NBC
          DO 60 J=1,NBC
           M=J+N6
60         Y(K,J)=BC(M,L)
100     CONTINUE
C
C  SAV4 is the central boundary condition array SAV2 modified by the
C    introduction of the e-parameter coefficients in SAV3
C
```

```
      DO 65 J=1,5
       SAV4(J,1)=SAV2(J,1)
       SAV4(J,3)=SAV2(J,3)
       SAV4(J,4)=SAV2(J,4)
   65  SAV4(J,2)=SAV2(J,2)-(EIG-1.)*SAV3(J)
      DO 70 K=N7,NDE
      J=K-2
      DO 70 M=1,N3
       L=M+N6
       Z(M,K)=SAV4(M,J)
       Z(M,J)=AA(L,K)
       IF(M.GT.NBC.OR.K.EQ.L) GO TO 70
       Z(M,J)=0.
   70  CONTINUE
      CALL SIMEQDD(Z,15,N3,NDE)
      CALL DETADD
  115 RETURN
      END
C
C                    *******    SIMEQDD    *******
C
C  SIMEQDD diagonalizes small arrays, specifically the 4x9 or 2x5 ones
C    from DET.  The diagonal elements, BIGA, are multiplied together to
C    obtain the determinant of the array.
C
      SUBROUTINE SIMEQDD(A,NA,NC,NR)
      COMPLEX*16 A(NC,NR),SAVE,BIGA,DETER
      DOUBLE PRECISION DETA,DETM
      INTEGER*2 IFLAG,IDEB
      COMMON /DETE/DETER,DETA,DETM,IFLAG
      COMMON /DEBUG/ IDEB
C
      DETER=(1.,0.)
      DO 25 J=1,NR
      J1=J+1
      BIGA=(0.,0.)
C
C  Here one finds the largest value in column J, to be called BIGA.
C
      DO 10 I=J,NR
      IF(CDABS(BIGA).GE.CDABS(A(J,I))) GO TO 10
      IA=I
      BIGA=A(J,I)
   10 CONTINUE
      DETER=DETER*BIGA
      IF(CDABS(BIGA).GT.1.D-33) GO TO 15
      DETER=(0.,0.)
      RETURN
C
C  Rearrange the rows such that the row with the largest first element
```

```
C     is at the top (to minimize roundoff errors when dividing through).
C
   15 DO 20 K=J,NC
      SAVE=A(K,J)
      A(K,J)=A(K,IA)
      A(K,IA)=SAVE
   20 A(K,J)=A(K,J)/BIGA
C
C  If a row exchange occurs, the sign of the determinant changes.
C
      IF (J.NE.IA) DETER=DETER*(-1.)
        END IF
      IF(J.EQ.NR) GO TO 30
C
C  Row reduction process:
C
      DO 25 I=J1,NR
      DO 25 K=J1,NC
   25 A(K,I)=A(K,I)-A(K,J)*A(J,I)
   30 J1=NR+1
      DO 35 I=2,NR
      M=NR+2-I
      IA=M-1
      DO 35 J=1,IA
      DO 35 K=J1,NC
   35 A(K,J)=A(K,J)-A(K,M)*A(M,J)
      RETURN
      END
C
C                      *******    DETADD    *******
C
C  DETADD converts the determinants of the small subarrays into polar
C    form and adds the angles and the log of the magnitude so as to
C    obtain the determinant for the entire array.
C
      SUBROUTINE DETADD
      COMPLEX*16 DETER
      REAL*8 DETERRE,DETERIM,DETA,DETM,AA1(2)
      INTEGER*2 IFLAG,IDEB
      EQUIVALENCE (DETER,AA1,DETERRE),(AA1(2),DETERIM)
      COMMON/DETE/DETER,DETA,DETM,IFLAG
      COMMON /DEBUG/ IDEB
      IF (CDABS(DETER).EQ.0.D00) THEN
        IFLAG=9
        GOTO 100
        END IF
      DETM = DETM + DLOG(CDABS(DETER))
      DETA = DETA + DATAN2(DETERIM,DETERRE)
  100 RETURN
      END
```

Appendix II: Symbols used

a = radiation density constant

B-V = colour index

c = speed of light

D = density

Dc = density at centre of star

g = gravitational acceleration

G = gravitational constant

H = mass of hydrogen atom

k = Boltzmann constant

M = mass

M_V = absolute visual magnitude

$M_\odot$ = mass of the sun

P = pressure

Pc = pressure at centre of star

R = radius

Rs = radius of star

S = entropy

t = time

T = temperature

Te = effective surface temperature

U = internal energy of a gas

V = visual magnitude

X = hydrogen abundance by mass

Xo = initial hydrogen abundance by mass

Y = helium abundance by mass

Yo = initial helium abundance by mass

Z = metal abundance by mass

Zo = initial metal abundance by mass

γ = ratio of specific heats c_p/c_v

ϵ = energy generation rate per unit mass

η = chemical potential of an element

κ = radiation absortion coefficient

μ = mean molecular weight of a gas

σ = Stefan-Boltzmann constant

τ = optical depth or eigenparameter

υ = exponent relating ϵ and T, as in $\epsilon \propto T^{\upsilon}$

ψ = measure of electron degeneracy

VITA

Surname: Von Rudloff Given Names: Ilmo Robert

Place of Birth: Saskatoon, Sask. Date of Birth: March 6, 1960

Educational Institutions Attended, with Dates of Entering and Leaving:

University of Saskatchewan, Saskatoon 1977 to 1978

University of Victoria, Victoria 1978 to 1985

Degrees, Diplomas, Etc., Awarded, with Dates and Names of Institutions:

B.Sc. (Honours) 1982 University of Victoria, Victoria

Honours and Awards:

N.R.C. Scholarship, 1982/83 and 1983/1984

Publications:

Ultraviolet Spectroscopy with IUE of OB Stars with Stellar Winds, J.B. Hutchings and I.R. Von Rudloff 1980, Ap.J., 238, 909.

A New Colour-Magnitude Diagram for the Peculiar Star Cluster E3 = C0921-770, J.E. Hesser, R.D. McClure, T.G. Hawarden, R.D. Cannon, I.R. Von Rudloff, B. Krueger, and D. Egles 1984, P.A.S.P., 96,406.

PARTIAL COPYRIGHT LICENSE

I hereby grant the right to lend my thesis (the title of which is shown below) to users of the University of Victoria Library, and to make single copies only for such users or in response to a request from the Library of any other university, or similar institution, on its behalf or for one of its users. I further agree that permission for extensive copying of this thesis for scholarly purposes may be granted by me or a member of the University designated by me. It is undertood that copying or publication of this thesis for financial gain shall not be allowed without my written permission.

Title of Thesis

The Thermal Stability of Hydrogen Burning Shells

Author 

Ilmo Robert Von Rudloff

September 1, 1985